Spring 5-10-2022

MULTIFUNCTIONAL CARBON-SUPPORTED COBALT-NICKEL COMPOUNDS FOR WATER SPLITTING AND ENERGY STORAGE APPLICATIONS

Wang Lin
Pittsburg State University, 1169203554@qq.com

MULTIFUNCTIONAL CARBON-SUPPORTED COBALT-NICKEL COMPOUNDS FOR WATER SPLITTING AND ENERGY STORAGE APPLICATIONS

A Thesis Submitted to the Graduate School
in Partial Fulfillment of the Requirements
For the Degree of
Master of Science

Wang Lin

Pittsburg State University

Pittsburg, Kansas

May 2022

MULTIFUNCTIONAL CARBON-SUPPORTED COBALT-NICKEL COMPOUNDS FOR WATER SPLITTING AND ENERGY STORAGE APPLICATIONS

Wang Lin

APPROVED:

Thesis Advisor _____
Dr. Ram Gupta, Department of Chemistry

Committee Member _____
Dr. Khamis Siam, Department of Chemistry

Committee Member _____
Dr. Serif Uran, Department of Physics

Acknowledgments

First, I would like to thank my supervisor, Dr. Ram Gupta, for his selfless guidance, commitment, professionalism, and dedication to my journey as a Master's student and a graduate research assistant. I have enjoyed working and learning from him on the day-to-day basis. I appreciate every opportunity he has presented to me, and I am grateful for the funding that enabled me to finish my second graduate degree.

Secondly, I would like to thank my family. Their continuous support allowed me to have a successful and stress-free study abroad. Special thanks to Dr. Khamis Siam and Dr. Serif Uran for participating in my thesis committee. I also thank Dr. Sarjay for assisting with XPS and SEM testing. I am grateful for the wonderful people and things available in this small town.

MULTIFUNCTIONAL CARBON-SUPPORTED COBALT-NICKEL COMPOUNDS FOR WATER SPLITTING AND ENERGY STORAGE APPLICATIONS

An Abstract of the Thesis by
Wang Lin

Hydrogen energy has high hopes as a representative of green energy in the pursuit of effectively reducing carbon emissions and mitigating climate change. According to the latest research, compounds of cobalt and nickel have been widely studied as alternatives to precious metals as catalysts for the electrolysis of water. Based on prior research, a hydrothermal method to grow cobalt-nickel hydroxide on pre-carbonized nickel foam was proposed. To compare the modification results of these materials by different activation methods, calcination, sulfidation, and phosphorization were performed on the materials. Among all the samples, the phosphorized material not only had superior performance compared to commercial materials in the catalytic reaction of hydrogen and oxygen evolution, but also exhibited satisfactory performance as an energy storage material for supercapacitor applications. In addition, an electrochemical synthesis method was used to simplify the synthesis of the cobalt-nickel compounds. The results show that the cobalt-nickel phosphide material derived from the electrochemical synthesis method has great potential in the field of flexible supercapacitors.

TABLE OF CONTENTS

LIST OF TABLES

LIST OF FIGURES

CHAPTER I

INTRODUCTION

To better respond to the energy crisis and solve environmental pollution problems, a consensus has been reached to reduce dependence on and use of fossil fuels [1][2][3]. Presently, the consumption of petroleum by automobiles accounts for half of the world's total petroleum extraction [4], making the development of alternatively fueled vehicles an effective way to significantly reduce dependence on fossil fuels [5]. Battery technology has reached a high level, and electric vehicles using lithium batteries as a power source have achieved mass production and occupy a certain market scale [6], but suffer several disadvantages such as the high weight of the battery, long charging time, short cruising range, and troublesome disposal of used batteries [7][8][9][10]. From the current consensus on the technical and theoretical limitations of these batteries, it is difficult to further improve performance to resolve these problems [11][12][13]. Instead, the energy storage devices that are expected to replace lithium-ion batteries as the power source of automobiles in the future include supercapacitors and hydrogen fuel cells [14][15][16][17].

1.1. Supercapacitors

Supercapacitors are an attractive class of energy storage devices that have both the advantages of batteries and capacitors [18]. Its distinguishing features are high power density, efficient charge-discharge performance, and ultra-long cycle life [19]. Based on these characteristics, supercapacitors have broad market application prospects, such as a power source for electric vehicles [20]. Efficient charging and discharging can remedy the long charging time of current electric vehicles, which enables their use in long-distance travel. In addition, a short charging time can boost the efficiency of charging stations and bring down their high construction costs. These advantages can promote the development and popularization of electric vehicles. Supercapacitors can be generally categorized into electric double-layer capacitors (EDLC) and pseudocapacitors based on their energy storage mechanisms [21].

1.1.1. Electric double layer capacitors

Electric double-layer capacitors are similar to capacitors in their energy storage mechanism. In the electrochemical system, they rely on the electric double layer generated by the electrostatic adsorption of charged ions on the surface of electrodes in the electrolyte to achieve charge storage. This is purely electrostatic adsorption and desorption process, without any redox process involved, and no charges pass through the electric double layer. In EDLCs, active materials commonly used include activated carbon materials, carbon fibers, and graphite. Compared with capacitors, the high specific capacitance of EDLCs come from the ultra-high specific surface area of the energy storage

material and the extremely small distance between the electric double layers. Typical features of electric double-layer capacitors are their high rate of performance as well as their long cycle life. This makes EDLCs suited to systems that require high-power pulses, such as elevators, forklifts, cranes, etc. However, the biggest problem that electric double-layer capacitors currently face is their low energy density, which means that electric double-layer capacitors are not suitable as a power source for electric vehicles because of their poor cruising range [22][23].

1.1.2. Pseudocapacitors

A pseudocapacitor relies on a high reversible redox reaction for its electrochemical function. In terms of reaction mechanisms, pseudocapacitors and rechargeable batteries have many similarities. Materials commonly used as pseudocapacitors include conductive polymers, transition metal compounds, and precious metals. Compared with electric double-layer capacitors, the most intuitive advantage of pseudocapacitors is their considerable energy density. As such, pseudocapacitors have the potential to replace lithium-ion batteries as a power source for electric vehicles [24][25][26].

1.2. Hydrogen energy

As an alternative to fossil fuels, green hydrogen energy is an ideal energy source to solve the current energy crises we face [27]. Vehicles powered by hydrogen fuel cells have great advantages over current electric vehicles. First, hydrogen fuel cell vehicles can achieve rapid refilling of hydrogen, and in addition, they have excellent endurance due to the high calorific value of hydrogen energy. The main factor limiting the development of hydrogen energy vehicles is the high cost of green hydrogen energy production. There are several methods to generate it, however, water electrolysis is the best method, which requires an eco-friendly means of electricity that could be generated from wind or solar energy [28][29][30]. Overall, this method can be a carbon-free and less toxic one. The main factors of the high cost of green hydrogen energy are electricity and water electrolysis catalysts. Catalysts play a crucial role in electrochemistry due to their ability to reduce the energy consumption for reactions. Hence, lots of research on efficient and low-cost electrocatalysts is the top priority for realizing the mass production of green hydrogen energy. The water electrolysis process includes two half-reactions, electrocatalytic hydrogen evolution and electrocatalytic oxygen evolution [31][32].

1.2.1. Hydrogen evolution reaction

The hydrogen evolution reaction (HER) occurs at the cathode of the electrolyzed water. Under acidic and alkaline conditions, the HER mechanism is basically the same, except that the source of protons differs. Under acidic conditions, the proton source is acid, and under alkaline conditions, the proton source is water. Taking acidic conditions

as an example, the reaction mechanisms of the hydrogen evolution reaction mainly fall into the following three categories: Volmer reaction, Heyrovsky reaction, and Tafel reaction [33].

The Volmer reaction and Heyrovsky reaction correspond to the electrochemical adsorption step and the electrochemical desorption step. The electron transfer allows the proton to gain electrons to form an adsorbed hydrogen atom, then the adsorbed hydrogen atoms combine with protons in the electrolyte. The third Tafel reaction belongs to the composite desorption step, and the hydrogen atoms adsorbed on the catalyst combine with each other to generate hydrogen gas. From the perspective of the reaction mechanism of the HER, the entire hydrogen evolution process can be divided into two steps: electron transfer and desorption. The kinetic process of the electrochemical reaction can be inferred from the magnitude of the Tafel slope. During the hydrogen evolution reaction, the adsorption and desorption of hydrogen atoms on the catalyst surface are a pair of competing reactions. If the adsorption is too strong, it is easy to form hydrogen, but it is not conducive to the discharge of hydrogen. If the adsorption is too weak, hydrogen formation is difficult but easier to discharge. When a good balance between adsorption and desorption is achieved, it can show good hydrogen evolution activity. Catalytic activity is usually characterized by the free energy of hydrogen adsorption (ΔG_H). The closer ΔG_H is to 0, the easier the hydrogen evolution reaction is. The relationship between the free energy of hydrogen adsorption and catalytic activity of several common metals shows a "volcanic" relationship [34][35].

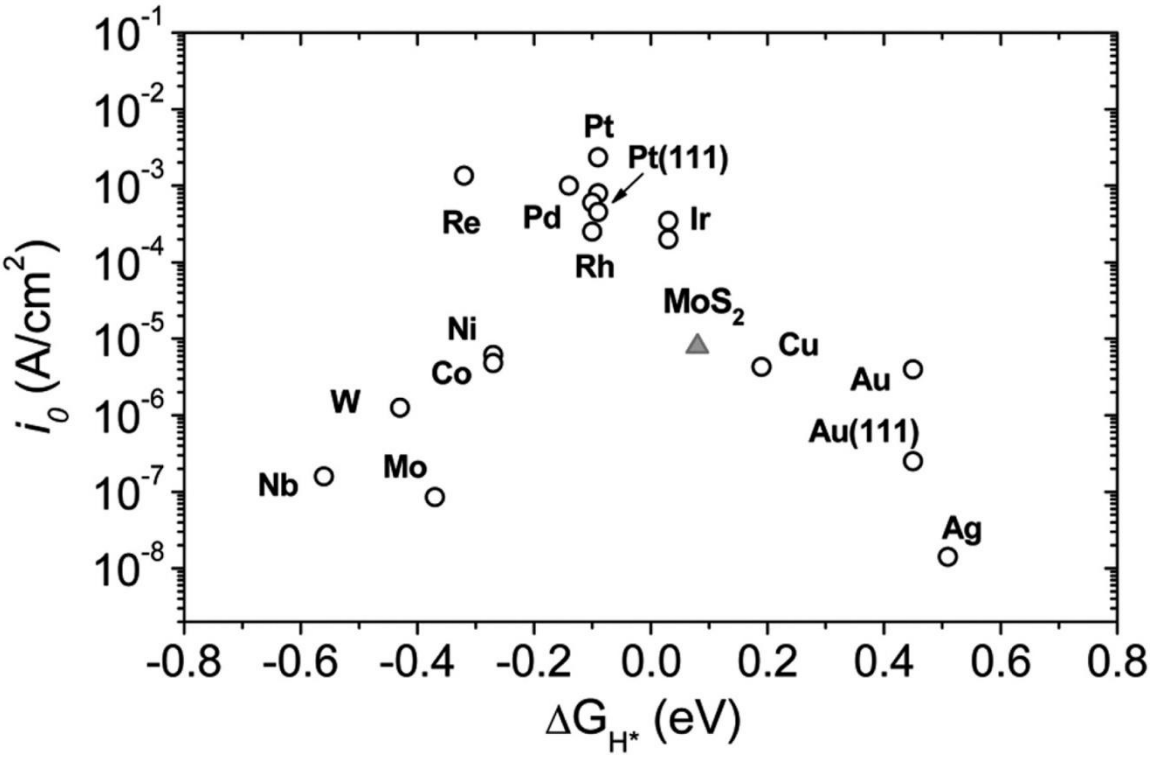

Figure 1.1. Trends in HER activity plot. Adapted with permission from [33]. Copyright 2014, American Chemical Society.

Among them, Pt-based precious metals have moderate hydrogen adsorption free energy, and experiments have also proved that they have high hydrogen evolution reaction rate and catalytic activity. However, Pt-based materials are not practical for large commercial use due to their rare and expensive nature. Therefore, it is important to explore catalysts with moderate hydrogen adsorption free energy, or optimize existing materials for this purpose.

1.2.2. Oxygen evolution reaction

The oxygen evolution reaction (OER) occurs at the anode of electrolyzed water. The OER process involves a multi-electron transfer process with a slow reaction rate and

high overpotential, which causes the high energy consumption of electrolyzed water and restricts the commercial development of electrolyzed water [36].

The reaction mechanism of OER is [37]:

In acidic electrolytes,

$M + H_2O \rightarrow M\text{-}OH + H^+ + e^-$

$M\text{-}OH \rightarrow M\text{-}O + H^+ + e^-$

$2M\text{-}O \rightarrow O_2 + 2M$

In alkaline electrolytes,

$M\text{-}O + OH^- \rightarrow MOOH + e^-$

$MOOH^- + OH^- \rightarrow M + O_2 + H_2O + e^-$

Where M represents a metal element which can produce metal-oxygen (M–O) intermediates in different electrolytes. These intermediates can form O_2 in two different ways. Two M-O intermediates can combine to produce O_2, or a M-OOH intermediate can form from which O_2 is produced. Oxygen evolution involves 4 electron transfers, and the kinetics of the M-O bond breaking are sluggish, which has a slowing effect on the anodic reaction of water electrolysis [38][39].

1.2.3. Research status of electrocatalysts

Presently, the best catalysts for hydrogen production from water electrolysis are still platinum-series precious metals, while RuO_2 and IrO_2 are still regarded as the best OER catalysts. However, these precious metals are naturally scarce, making them expensive and therefore not suitable for large-scale commercial electrocatalysts. Aside

from precious metals, the following types of materials have also been widely studied as catalysts for water electrolysis:

(1) Transition metal oxides [40][41], hydroxides [42], phosphides [43], sulfides [44], etc.

(2) Transition metal alloys [45].

(3) The transition metal/metal compound is supported by carbon-based materials [46][47].

1.3. Content and motivation for the selection of this project

Based on previous studies, we confirmed that cobalt-nickel oxides have great potential in both energy storage and water electrolysis catalysis. In the previous stage of research, we investigated the electrochemical characteristics of cobalt-nickel oxide and cobalt-nickel oxide polyaniline composites. In addition, we found that the activated carbon material prepared with polyaniline as a precursor has good electrochemical properties including its outstanding electrochemical stability. Based on previous research results and others' reports on cobalt-nickel compounds, the target of our work was an investigation on how to combine carbon materials with cobalt-nickel compounds to obtain cobalt-nickel compound-carbon composites with better electrochemical performance. Carbon-supported metal nanoparticles have a high loading and high dispersibility, which are very beneficial for the construction of ultrathin catalyst layers. We determined the research method for the synthesis of carbon-supported cobalt-nickel compounds and their electrochemical properties. In the quest to come up with high-performance electrodes or electrocatalysts, carbon supports need to have the following

characteristics: high specific surface area to obtain maximum active sites, high conductivity to minimize voltage drop due to system internal resistance, and high corrosion resistance to achieve better electrochemical stability [47][48]. Currently, widely used carbon supports are carbon cloth, carbon nanotubes, carbon black, graphene, etc. In this work, we used two different substrates which consisted of carbon cloth and nickel foam with a carbon precursor layer. In the first part of the work, nickel foam with a carbon precursor layer was used as the substrate, and the hydrothermal method was adopted to obtain carbon-based cobalt-nickel compounds. In addition, different samples were calcined, sulfurized and phosphorized to analyze the effect of different techniques on the electrochemical characteristics of carbon-based cobalt-nickel compounds. In the second part of the work, carbon cloth was used as the substrate and obtained the cobalt-nickel compound was uniformly deposited on the carbon cloth by electrochemical synthesis. Likewise, different samples were calcined, sulfurized, and phosphorized to investigate whether their electrochemical performance was improved.

CHAPTER II

EXPERIMENTAL DETAILS

2.1. Materials

The chemicals obtained for the synthesis of the electrodes tested in this experiment were used as such and supplied from the following companies: nickel foam from MTI-KJ Group, Richmond California, glucose from Acros, New Jersey, USA, urea 98% from Acros, New Jersey, USA. The purity of both $Co(NO_3)_2 \cdot 6H_2O$ and $Ni(NO_3)_2 \cdot 6H_2O$ were 99% and from Strem Chemicals, Newburyport. Na_2S nonahydrate from Acros Organics, USA, and $H_2NaPO_2 \cdot H_2O$ 99% from Aldrich, Milwaukee, Wisconsin, USA.

2.2. Hydrothermal synthesis of cobalt-nickel compounds on nickel foam with a carbon precursor layer

In this part of the work, a hydrothermal method was used for the synthesis of cobalt-nickel compounds on substrates. Four samples were synthesized and were labeled as $Co_2Ni(OH)_8$@C, Co_2NiO_4@C, Co_2NiS_X@C, and Co_2NiP_X@C for the hydroxide, calcined, sulfurized, and phosphorized samples, respectively.

The first step was the synthesis and modification of the substrate. The carbon precursor was formed on the Ni-foam through a hydrothermal method. 3 mmol of glucose

was dissolved in 20 mL of distilled water for each 40 mL reactor. The reactor was sealed with Teflon tape before the reactors were placed in an oven. The reaction took 12 hours at 180 °C. This process was completed for four pieces of Ni-foam. The obtained carbon-encapsulated nickel foams were rinsed with distilled water and placed under sonication in isopropanol for approximately one minute to remove any loose particles. Then the samples were calcined at 500 °C for 2 hours (the temperature was brought up by 5 °C/min) under an inert N_2 atmosphere.

Afterward, the samples underwent the addition of the transition metal hydroxide through another hydrothermal method. The following compounds and amounts were added to a beaker, 20 mL of distilled water, 2 mmol of $Co(NO_3)_2{\cdot}6H_2O$, 1 mmol of $Ni(NO_3)_2{\cdot}6H_2O$, and 0.06 g of urea and dissolved. The substrate synthesized in the previous step and prepared solution were transferred to the reactor, after which they were sealed and placed in a thermostatic oven for 12 hours at 140 °C. Afterward, the samples were rinsed with isopropanol and dried. The four foam pieces were treated differently. One $Co_2Ni(OH)_8$@C piece remained unmodified, another was calcined at 350 °C for two hours, the third sulfurized, and the final phosphorized.

The sulfurization of the third sample was achieved via a solvothermal method through the addition of Na_2S. One of the $Co_2Ni(OH)_8$@C samples was placed in the bottom of the reactor with an additional 700 mg of Na_2S and 20 mL of distilled water. After the vessel was sealed it was placed in the autoclave oven for 24 hours at 140°C. The sample was then rinsed with isopropanol and dried.

One of the $Co_2Ni(OH)_8$@C samples was phosphorized in a tube furnace under an inert argon atmosphere for 2 hours at 320°C. The electrode sample was placed in an open quartz vessel and the $H_2NaPO_2{\cdot}H_2O$ was placed in a second vessel. The vessels were placed inside the oven in the middle of the length of the flow tube with the phosphorus material closest to the flow source and the electrode sample vessel approximately 1 cm from the end of the first vessel. Enough $H_2NaPO_2{\cdot}H_2O$ was added to the first vessel to achieve a 10:1 ratio with the deposited mass of Co_2NiO on the electrode, which required the use of 333.5 mg of $H_2NaPO_2{\cdot}H_2O$.

2.3. Electrochemical synthesis of cobalt-nickel compounds on carbon cloth

In electrochemical synthesis, a three-electrode system was used to synthesize cobalt-nickel compounds. First, the following compounds and amounts were added to a beaker to make an electrolyte, 20 mL of distilled water, 2 mmol of $Co(NO_3)_2{\cdot}6H_2O$, 1 mmol of $Ni(NO_3)_2{\cdot}6H_2O$, and 0.06 g of urea and dissolved. A cleaned carbon cloth was used as the working electrode. Ag/AgCl and a platinum sheet served as reference electrode and counter electrode. Chronopotentiometry testing was done at -1 V for 20 minutes. A VersaSTAT 4-500 electrochemical workstation (Princeton Applied Research, Oak Ridge, TN, USA) was used to do the electrodeposition. The obtained carbon cloth with the uniformly grown cobalt-nickel compound was rinsed with DI water before being placed in an oven at 70 °C for 12 hours to dry.

The dried cobalt-nickel-carbon cloth compound was calcined, sulfurized, and phosphorized, consistent in operation with the modifications done to the hydrothermal samples obtained in the previous step.

2.4. Material characterization

2.4.1. Scanning electron microscope

Scanning electron microscopy (SEM) can intuitively provide the microscopic morphology of synthetic materials, which can help to compare the structure of materials synthesized by different methods. In addition, SEM images can be used in the interpretation of the specific properties of the material. For example, for electric double layer capacitors, the microscopic morphology of the energy storage material has a direct impact on its electrochemical performance; the more abundant the pore structure, the higher the specific capacitance. In addition, SEM results can be used to reinforce the result of another testing method. For example, the SEM results can corroborate the BET results to explain the high specific surface area and abundant pore structure of the material. Quanta 200 SEM (FEI, Hillsboro, Oregon, USA) was used to obtain the SEM image of all synthetic materials.

2.4.2. X-ray photoelectron spectroscopy

X-ray photoelectron spectroscopy (XPS) is one of the most important technical means for qualitative and quantitative analysis of synthetic materials. First, by obtaining the elements in the composite material through the XPS test, it can be confirmed whether the target elements are present in the composite material. More importantly, the precise

measurement of the chemical shifts of the electron binding energy of the inner shell by XPS, can provide information on the chemical bonds used to confirm the structure of the compound.

The chemical composition of the synthesized samples was determined via XPS analysis. A ThermoFisher Scientific Instruments analyzer (East Grinstead, UK) was used to perform the X-ray photoelectron spectroscopy.

2.5. Electrochemical testing

To reveal the electrochemical performance of all synthesized materials for energy storage in supercapacitors and catalysts for water electrolysis, a VersaSTAT 4-500 electrochemical workstation (Princeton Applied Research, Oak Ridge, TN, USA) was used. The three-electrode testing system was used to evaluate all electrochemical performance. For both the energy storage and catalytic performance tests, the synthesized sample was used as the working electrode, and the platinum wire was used as the counter electrode. The test differ in electrolyte and reference electrode. For the energy storage test, 3 M KOH solution and Hg/HgO served as the electrolyte and reference electrode, respectively. For the electrocatalytic tests, 1 M KOH solution and Saturated Calomel Electrode served as electrolyte and reference electrode, respectively.

2.5.1. Cyclic voltammetry

Cyclic voltammetry (CV) is a commonly used method to reveal the electrochemical properties of materials. The potential-current curve is recorded by scanning through a range of voltages and measuring the current. The potential-current curve recorded by cyclic voltammetry can determine whether the material has redox characteristics. There are two typical characteristic curves of CV: the first one is quasi-rectangular, usually, the CV curve of carbon materials without redox characteristics is quasi-rectangular, which is also the typical characteristic CV curve of electric double layer capacitor materials. The second is the duck shape, usually the CV characteristic curve exhibited by pseudocapacitive materials. Furthermore, the same material is subjected to different scan rates to study its reversibility. Usually, at different scan rates, the peak potential of the material is fixed, but the reversibility of the material is stronger, which is also the key to achieving high charge-discharge efficiency of supercapacitors.

2.5.2. Galvanostatic charge-discharge

As one of the most important parameters to measure the performance of supercapacitors, specific capacitance can usually be obtained from the test results of cyclic voltammetry or the Galvanostatic charge-discharge (GCD) method. In this project, we choose the Galvanostatic charge-discharge test results to calculate the specific capacitance of the composite materials through Equation 1.

$$C_{sp} = \frac{i \times \Delta t}{\Delta V} \quad \ldots\ldots (1)$$

Where: C_{sp} is specific capacitance (mF/cm^2), i is discharge current density (mA/cm^2), Δt is discharge time (s), and ΔV is the potential window for discharge.

In addition, to study the rate performance of the material, different charge-discharge current densities from 30 mA/cm^2 to 0.5 mA/cm^2 were used to obtain the charge-discharge test data of the material. The corresponding specific capacitance was calculated through Equation 1. Generally, the material has a good rate performance when the material has a close specific capacitance under high or low charge-discharge current density. Good rate performance is the key to achieving high charge and discharge efficiency of the material.

Energy density is one of the important parameters that determines the use of supercapacitors, which can be calculated from the test data of charge and discharge.

$$E = C_{sp} \times (\Delta V)^2/7200 \quad \ldots\ldots (2)$$

Where: E is energy density (Wh/cm^2), C_{sp} is specific capacitance (F/cm^2), and ΔV is the potential window for discharge.

2.5.3. Electrochemical impedance spectra

Electrochemical impedance spectroscopy (EIS) is a method of measuring the impedance of the working electrode in a three-electrode system. The AC impedance method studies the electrode system by means of the impedance spectrum over a wide frequency range. The electrode conductivity is obtained by measuring the semicircle diameter of the fitted impedance spectrum of the electrochemical impedance. The smaller the resistance, the better the electrode conductivity. The better the conductivity

of the electrode, the faster the electron transfer, and the better the electrochemical performance of the material.

2.5.4. Cycle performance test

The electrochemical stability of supercapacitors was obtained by 5000 cycles charge-discharge test. The stability of the material used for supercapacitor energy storage is determined by the change of specific capacitance with the increase of charging-discharging number of times. The slower the specific capacitance decays, the better electrochemical stability. In addition, the Coulombic efficiency of the material, the percentage of discharge specific capacity and charge specific capacity, can also be obtained by 5000 charge-discharge cycles.

2.5.5. Linear sweep voltammetry (LSV)

Overpotential is one of the most important indicators to measure the activity of water electrolysis catalysts. In this work, overpotential refers to the difference between the actual voltage and the theoretical voltage required during the catalytic reaction when the catalytic reaction reaches a specific current density. Usually, the overpotential can be determined by linear sweep voltammetry (LSV). In addition, the LSV polarization curve can intuitively reflect the change of current density with applied voltage. Generally, in order to increase the current density, it is necessary to increase the applied voltage. The smaller increases in overpotential resulting in larger increases in current density is desired. Here the Tafel slope is defined, as the rate at which the current increases concerning for to the overpotential. The Tafel slope is not only an important parameter

to reveal the catalytic reaction mechanism, but also an important criterion to measure the quality of the catalyst. In addition, the electrochemical stability of the catalyst material can also be determined by comparing the multiple LSV test. If the polarization curve obtained after thousands of LSV scans does not have a large displacement or even basically coincides with the initial polarization curve, it can be determined that the material has good electrochemical stability.

2.2.6 Chronoamperometry

Chronoamperometry or chronopotentiometry can be used to assess catalyst stability. Chronoamperometry records the change of current through the electrode over time by applying a specific constant voltage to the system. The smaller the current decay, the better the electrocatalytic stability. Chronopotentiometry is similar, except the current is held constant, and the potential measured.

CHAPTER III

RESULTS AND DISCUSSIONS

3.1. Structure and morphology characterization

3.1.1. X-ray photoelectron spectroscopy

To confirm the composition of synthesized materials, X-ray photoelectron spectroscopy (XPS) was performed to demonstrate the existence of Ni, Co, S, and P elements. Figures 3.1.-3.8. show the XPS spectra of materials synthesized by hydrothermal and electrochemical methods. The peaks at 793.7 and 852.6 eV are characteristic of metallic cobalt and nickel, respectively, and are present in the XPS of all synthesized samples; which confirms that all synthetic compounds contain cobalt and nickel. In addition, the carbon layer or carbon cloth as the substrate also showed corresponding carbon peaks in the XPS spectrum. For both sulfurized materials, Co_2NiS_X@C (Figure 3.3) and Co_2NiS_X (Figure 3.7), the S 2p peak was detected at 164.0 eV, underscoring the successful synthesis of transition metal sulfides. Co_2NiP_X@C and Co_2NiP_X are two phosphorized samples, and their XPS spectra are shown in Figure. 3.4 and Figure. 3.8, respectively. The P 2p peak is located at 131.4 eV, which is typical transition metal phosphides [49][50].

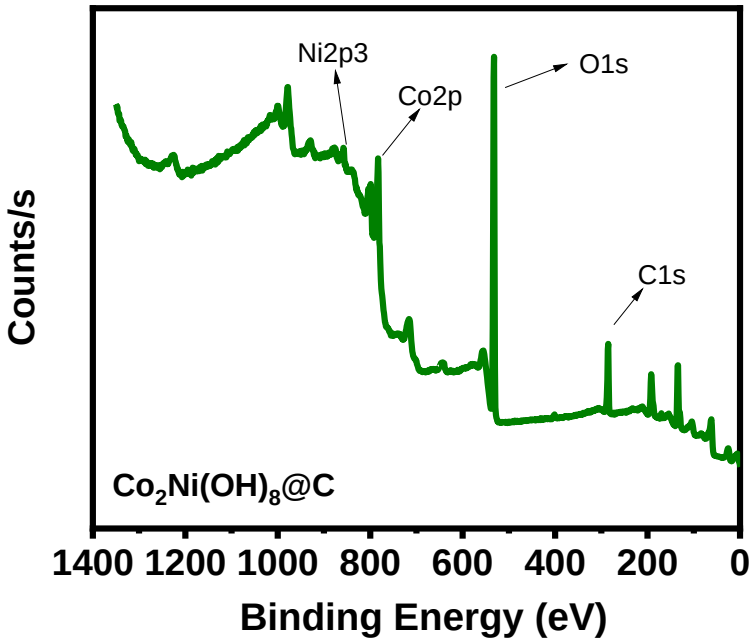

Figure 3.1. XPS spectra of $Co_2Ni(OH)_8$@C.

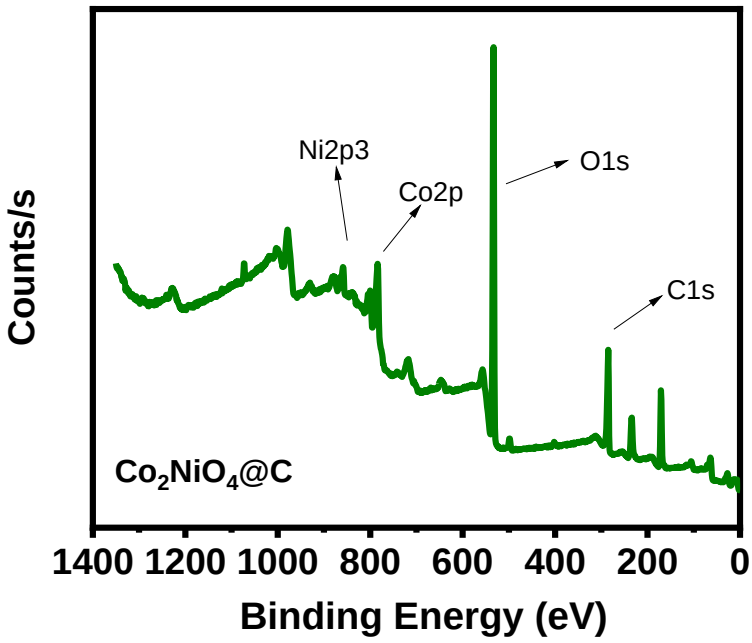

Figure 3.2. XPS spectra of Co_2NiO_4@C.

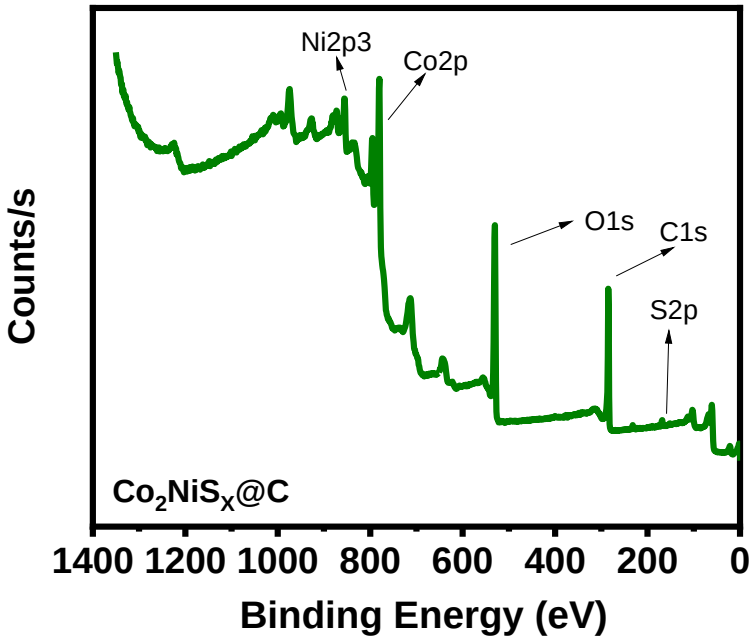

Figure 3.3. XPS spectra of Co_2NiS_X@C.

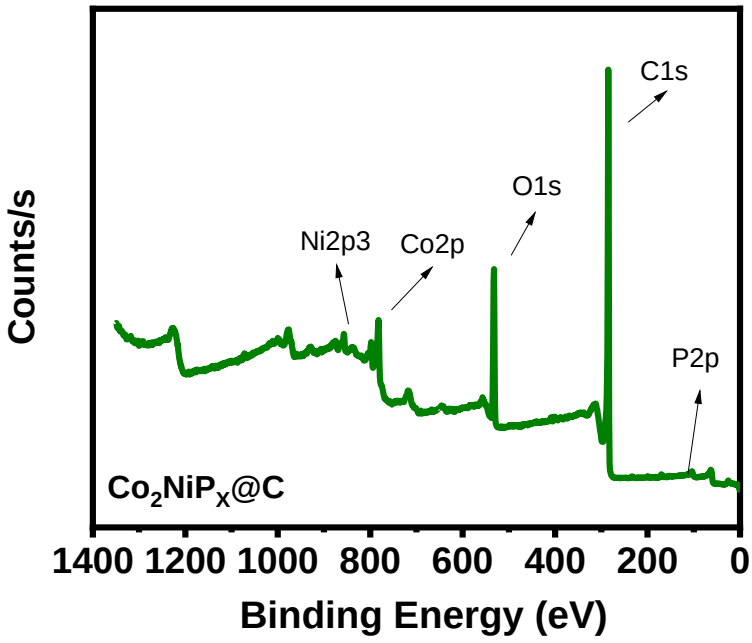

Figure 3.4. XPS spectra of Co_2NiP_X@C.

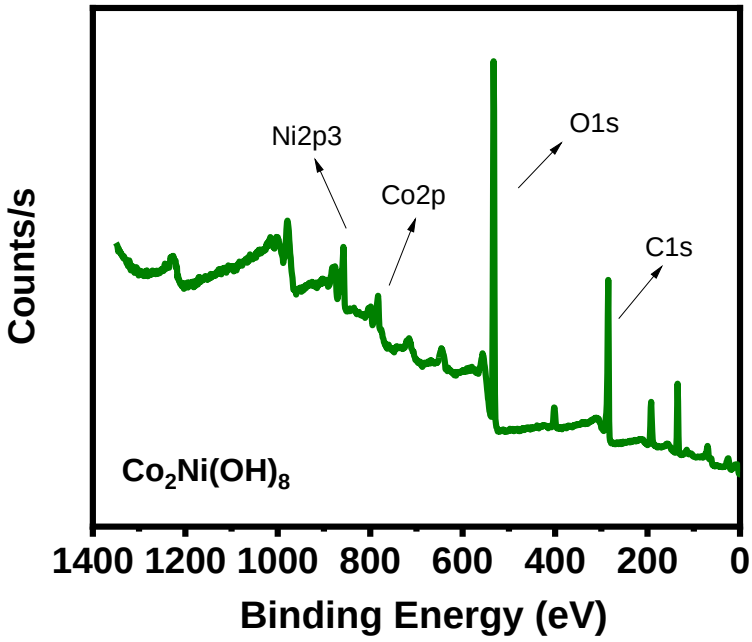

Figure 3.5. XPS spectra of $Co_2Ni(OH)_8$.

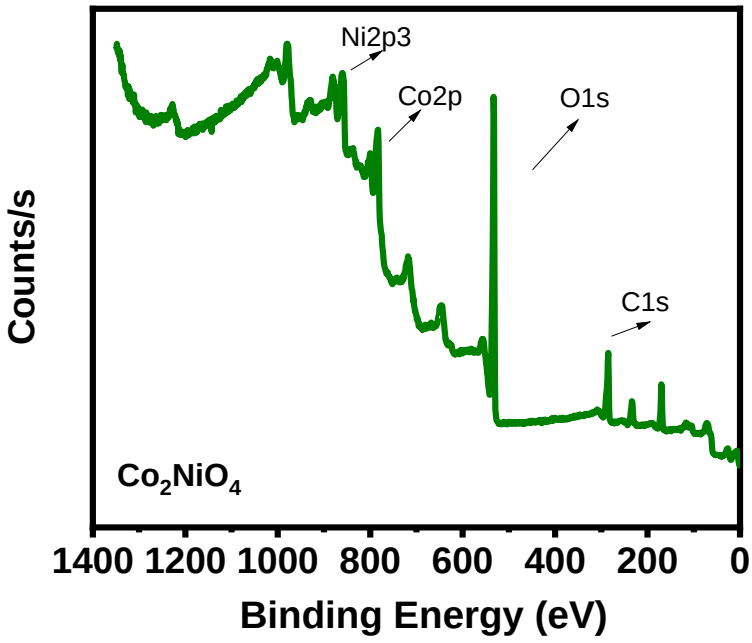

Figure 3.6. XPS spectra of Co_2NiO_4.

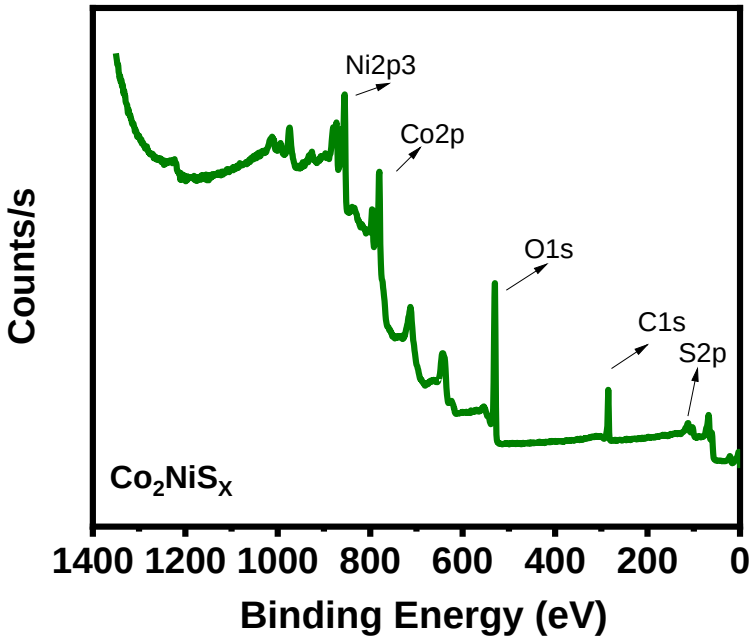

Figure 3.7. XPS spectra of Co_2NiS_X.

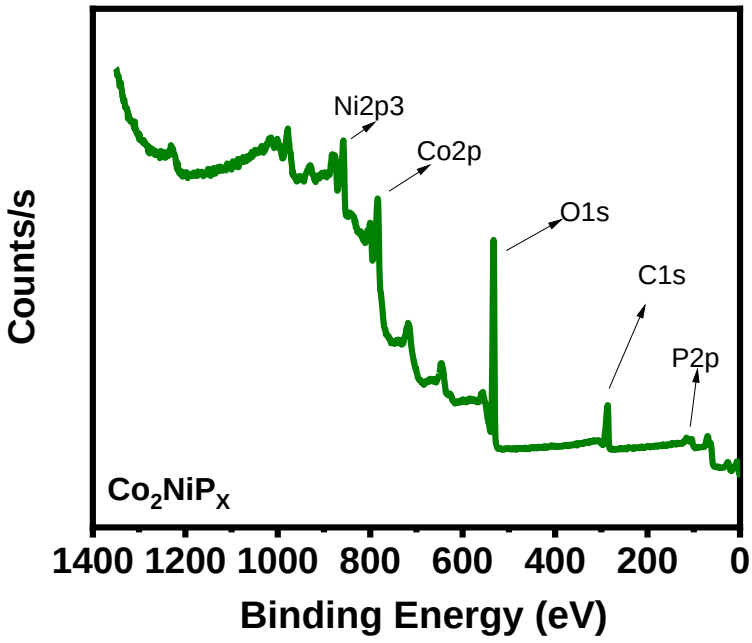

Figure 3.8. XPS spectra of Co_2NiP_X.

3.1.2. Scanning Electron Microscope images

The scanning electron microscopy image of all synthetic materials are shown in Figures 3.9-3.16. Figure 3.9 reveals the microscopic morphology of $Co_2Ni(OH)_8$@C synthesized by the hydrothermal method, which shows Sea urchin-like particles with clearly visible cores with particle sizes of 4-6 μm. The morphology of Co_2NiO_4@C obtained after further high-temperature calcination of $Co_2Ni(OH)_8$@C has changed greatly into a network shape, which is shown in figure. 3.10. The morphology of the Co_2NiS_X@C has also undergone great changes, and the surface is uneven and cracked (Figure 3.11). Figure 3.12 shows the Co_2NiP_X@C obtained by phosphorizing, which shows a vertical scale-like structure. The electrochemically synthesized $Co_2Ni(OH)_8$ (Figure. 3.13) is significantly different from the hydrothermally synthesized $Co_2Ni(OH)_8$@C (Figure. 3.9), showing fine vertical scale-like with some uneven particles. Co_2NiO_4 obtained by high-temperature calcination (Figure. 3.14) showed a scaly surface and some cracks. The Co_2NiS_X (Figure. 3.15) obtained by sulfurization showed a microscopic morphology similar to dry moss. Figure. 3.16 reveals the microstructure of Co_2NiP_X obtained by electrochemical method. It has a very similar microscopic morphology to Co_2NiP_X@C obtained by hydrothermal synthesis, with a vertical scale-like shape. It is worth noting that there are some cracks on the surface of the materials synthesized by the electrochemical synthesis method.

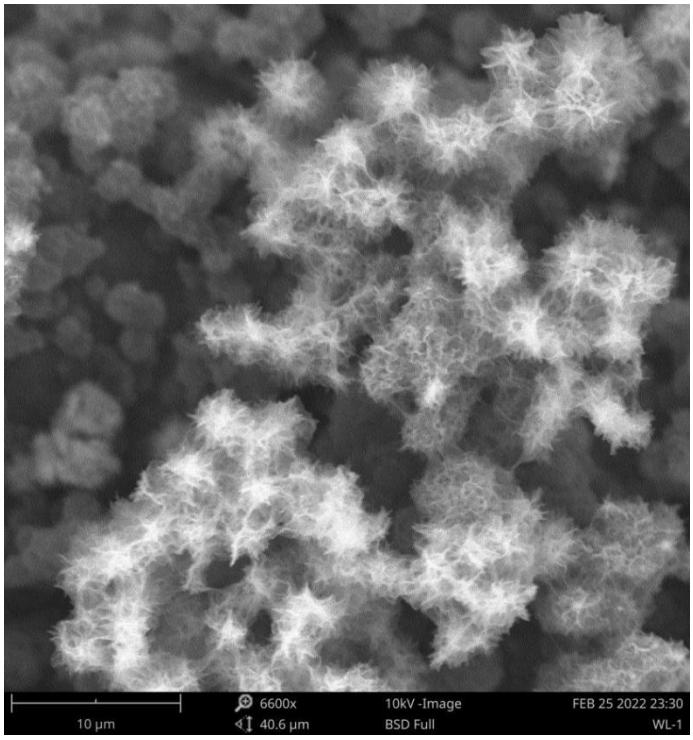

Figure 3.9. SEM image of $Co_2Ni(OH)_8$@C.

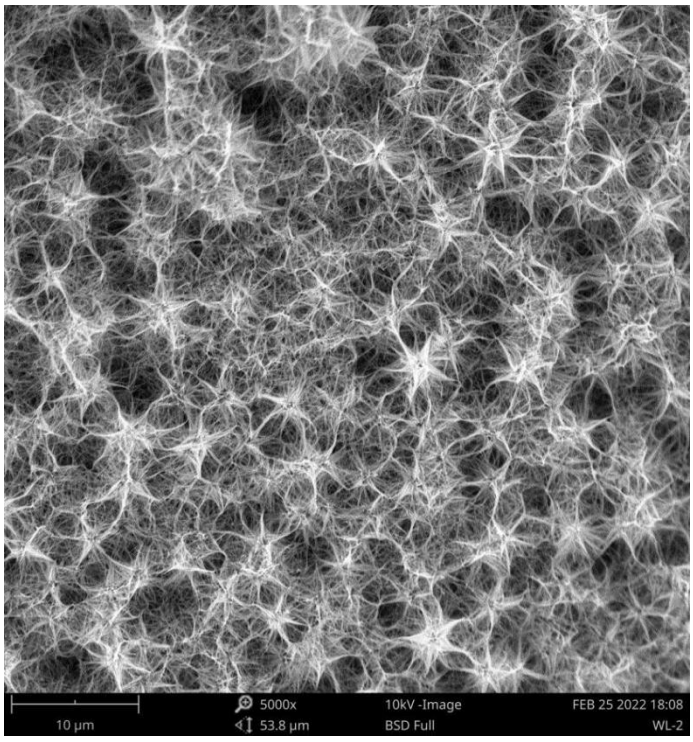

Figure 3.10. SEM image of Co_2NiO_4@C.

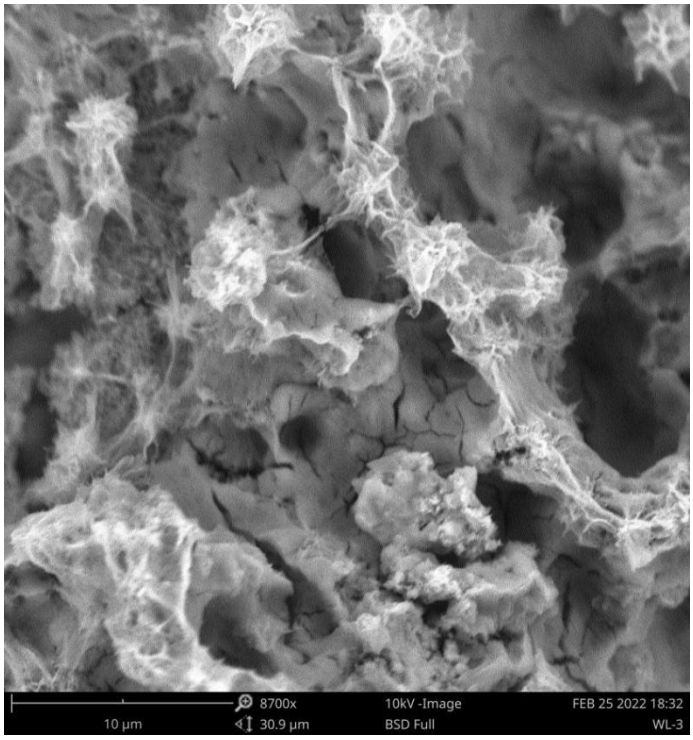

Figure 3.11. SEM image of Co_2NiS_X@C.

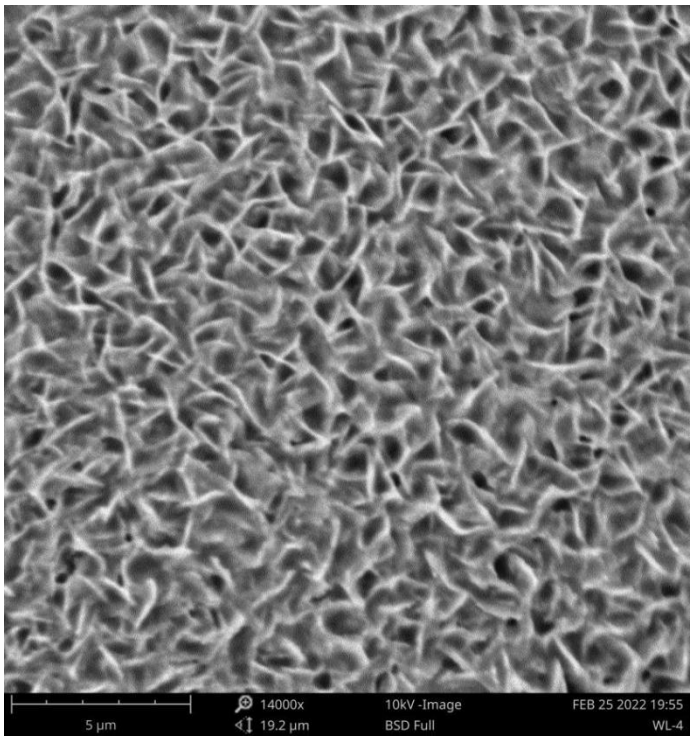

Figure 3.12. SEM image of Co_2NiP_X@C.

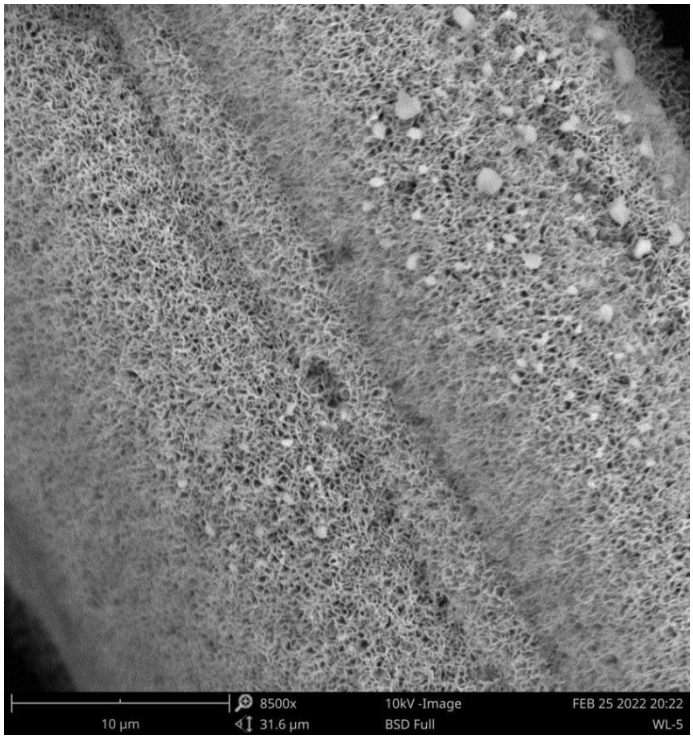

Figure 3.13. SEM image of $Co_2Ni(OH)_8$.

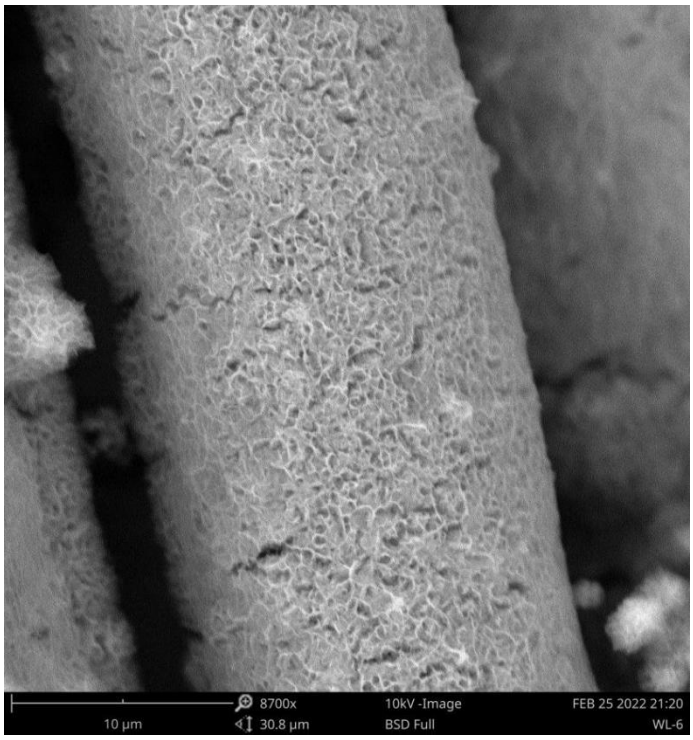

Figure 3.14. SEM image of Co_2NiO_4.

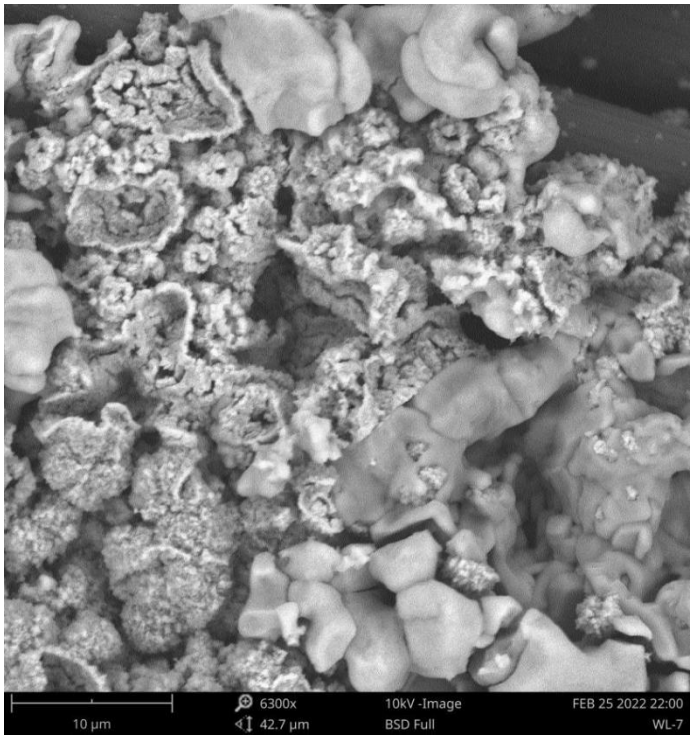

Figure 3.15. SEM image of Co_2NiS_X.

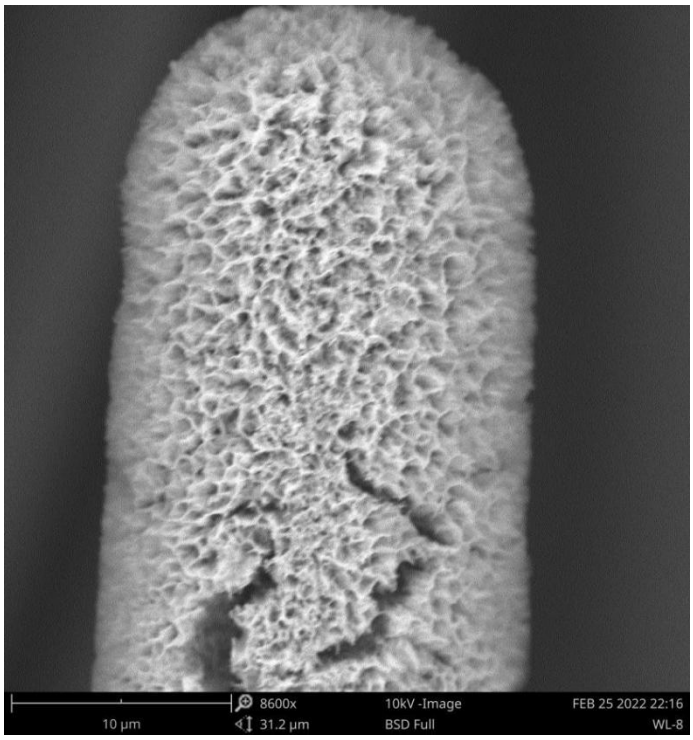

Figure 3.16. SEM image of Co_2NiP_X.

3.2 Electrochemical characterization

In this part of the work, we investigate the electrochemical properties of all samples through a three-electrode test system.

3.2.1 Electrochemical characterization of Co-Ni compounds supported on activated carbon

3.2.1.1. Hydrogen evolution reaction testing

The linear sweep voltammetry and cyclic voltammetry (LSV-CV) test was placed in 1M KOH electrolyte to investigate the HER activity of all synthesized samples with a scan rate of 2 mV/s. All synthesized samples, $Co_2Ni(OH)_8$@C, Co_2NiO_4@C, Co_2NiS_X@C, and Co_2NiP_X@C were tested under the same conditions and plotted in Figure 3.17. $Co_2Ni(OH)_8$@C exhibited an overpotential of 198 mV to reach a current density of 10 mA/cm^2. To its detriment, the overpotential of the calcined material increased to 218 mV, mainly because the high-temperature treatment greatly destroys carbon support layer. The overpotential of the sulfurized sample, Co_2NiS_X@C, was reduced to 153 mV at 10 mA/cm^2. Most notably, Co_2NiP_X@C showed an extremely low overpotential, which is 48 mV at 10 mA/cm^2. The Tafel slope describes the rate of increase in current density as the voltage increases, and a smaller Tafel slope means smaller kinetic barriers and faster reaction rates. A lower overpotential means a smaller voltage load to realize the water electrolysis reaction, and a lower Tafel slope means a faster electrolysis water reaction rate. Low overpotentials and low Tafel slopes are hallmarks of excellent water electrolysis catalysts, emphasizing low energy consumption for water electrolysis catalysis.

$Co_2Ni(OH)_8$@C, Co_2NiO_4@C, Co_2NiS_X@C, and Co_2NiP_X@C showed 131, 128, 154, and 68 mV/dec respectively (Figure 3.18). The HER catalytic activity of Co_2NiP_X@C is comparable to platinum-based materials, because Co_2NiP_X@C not only has a low overpotential, but also has fast reaction kinetics.

Electrochemical stability is an important criterion for the quality of electrocatalyst materials in addition to overpotential, Tafel slope, and internal resistance. Good electrochemical stability is the key to ensuring the commercial viability. In the HER test, to study the electrochemical stability of the material, 1000 cycles of LSV were tested, and the initial LSV polarization curve and the 1000 cycle LSV polarization curve were compared to obtain the electrochemical stability of the material. Figure 3.20 shows that after the Co_2NiP_X@C has undergone 1000 LSV cycles, the electrochemical performance of the material has slightly degraded since the polarization curve of the 1000th does not overlap with the initial.

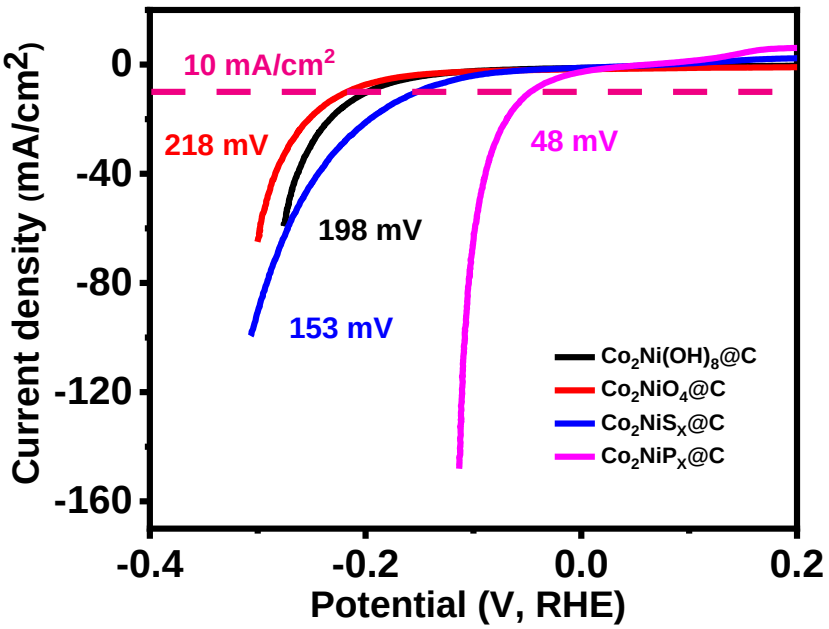

Figure 3.17. LSV-CV curves of $Co_2Ni(OH)_8$@C, Co_2NiO_4@C, Co_2NiS_X@C and Co_2NiP_X@C for HER.

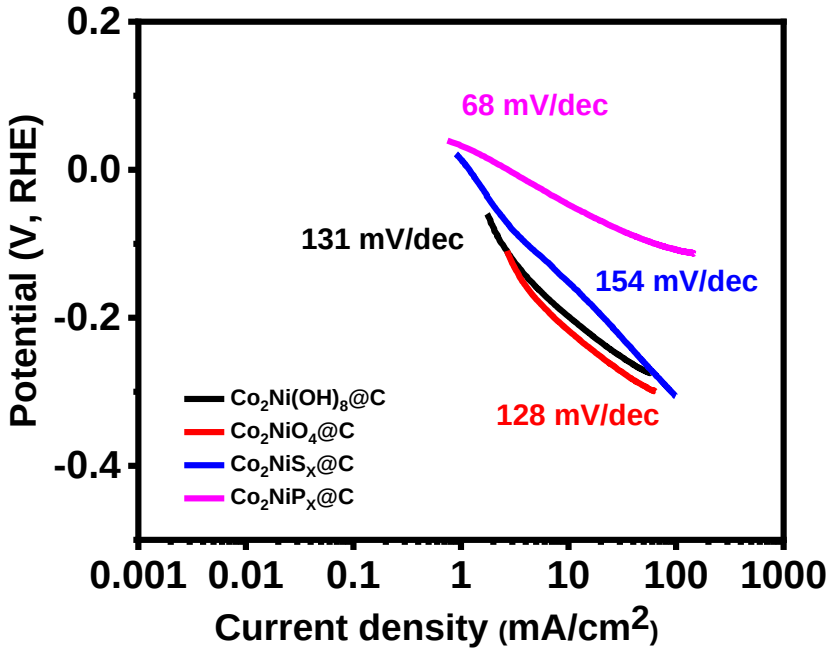

Figure 3.18. Corresponding Tafel curves for $Co_2Ni(OH)_8$@C, Co_2NiO_4@C, Co_2NiS_X@C and Co_2NiP_X@C.

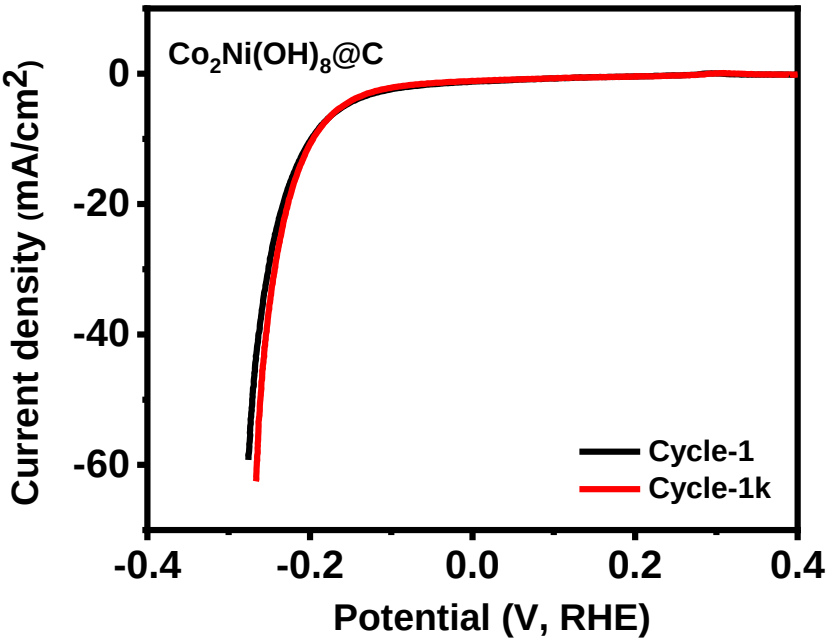

Figure 3.19. LSV-1 & LSV-1k HER stability test of the $Co_2Ni(OH)_8$@C.

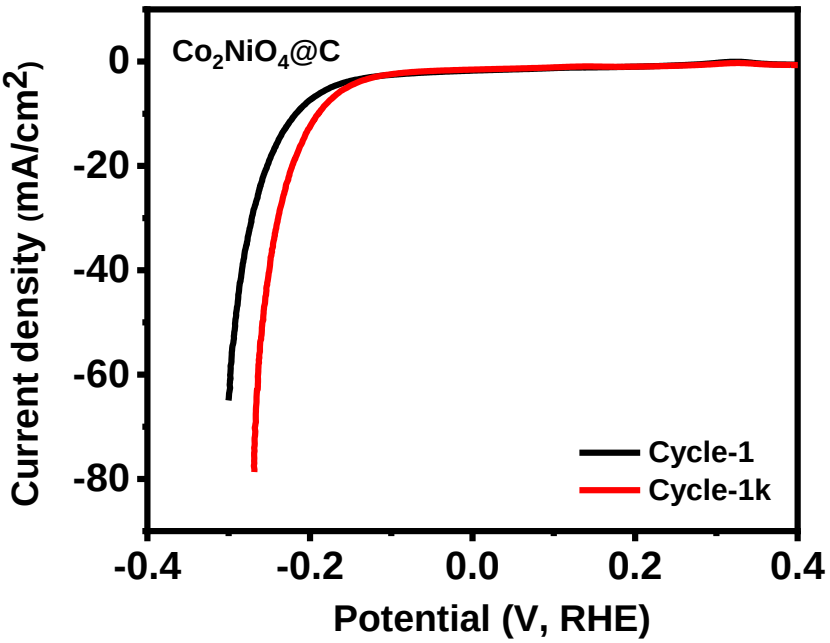

Figure 3.20. LSV-1 & LSV-1k HER stability test of the Co_2NiO_4@C.

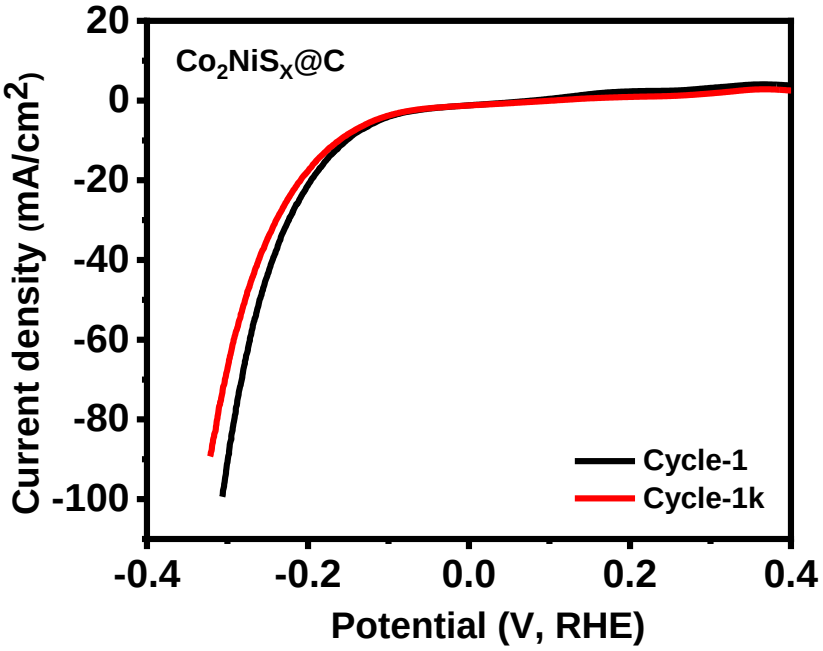

Figure 3.21. LSV-1 & LSV-1k HER stability test of the Co_2NiS_X@C.

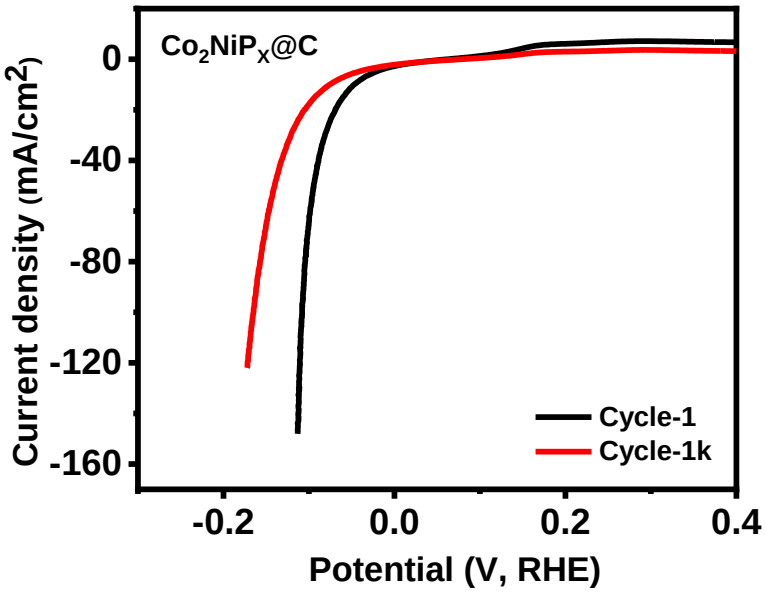

Figure 3.22. LSV-1 & LSV-1k HER stability test of the Co_2NiP_X@C.

Co_2NiP_X@C showed excellent HER performance. This result is not only superior to similar work, but also comparable to precious metal-based materials (Table 1).

Table 1. Summary of HER overpotentials of cobalt-nickel metal compounds

Similar work	Electrolyte	Overpotential	Tafel slope	References
$NiCo_2O_4$@C@NF	1 M KOH	42 mV	65 mV/dec	[47]
CoNiP@LDH	1 M KOH	83 mV	80 mV/dec	[50]
CoNiP/CC	1 M KOH	62 mV	88.3 mV/dec	[51]
Ni-Co-S-P	1 M KOH	78 mV	89 mV/dec	[52]
NiCoMo	0.1 M KOH	132 mV	108 mV/dec	[53]
NiCoP/CoP	1 M KOH	73 mV	91.3 mV/dec	[54]
Co/Co_3O_4	1 M KOH	90 mV	44 mV/dec	[55]
Co/CoO_X	1 M KOH	61 mV	78 mV/dec	[56]
NV-Ni/CP	1 M KOH	95 mV	140 mV/dec	[57]
Cu@Ni	1 M KOH	140 mV	79 mV/dec	[58]
β-Ni2P2O7/Pt	1 M KOH	28 mV	32 mV/dec	[59]
Pt/C	1 M KOH	38 mV	31 mV/dec	[2]
Co_2NiP_x@C	1 M KOH	48 mV	68 mV/dec	This work

3.2.1.2. Oxygen evolution reaction testing

The OER characteristics of these materials were also studied. OER involves a complex electron transfer process with slow reaction kinetics and therefore high overpotential, which is a key factor that limits the efficiency of water electrolysis. The LSV-CV test results show that the overpotential of $Co_2Ni(OH)_8$@C is 348 mV to achieve a current density of 10 mA/cm^2 (Figure 3.23). The overpotential of the Co_2NiO_4@C obtained after calcination has risen to 403 mV when the current density is 10 mA/cm^2. Compared to $Co_2Ni(OH)_8$@C, the overpotential of the sulfurized and phosphorized materials are reduced to 341 mV and 332 mV respectively. As an indicator of reaction kinetics, the Tafel slopes of $Co_2Ni(OH)_8$@C, Co_2NiO_4@C, Co_2NiS_X@C, and Co_2NiP_X@C were calculated by the

Tafel slope formula, which figured out to be 95, 63, 76, and 73 mV/dec, respectively (Figure 3.24).

To understand the electrochemical performance of these synthesized samples as OER catalysts, the comparison table of OER test results with those of precious metal-based OER catalysts and other similar works is as follows:

Table 2. Summary of OER overpotentials of cobalt-nickel metal compounds

Similar work	Electrolyte	Overpotential	Tafel slope	References
$NiCo_2O_4$@C@NF	1 M KOH	242 mV	86 mV/dec	[47]
CoNiP@LDH-100	1 M KOH	216 mV	45 mV/dec	[50]
CoNiP/CC	1 M KOH	242 mV	109.8 mV/dec	[51]
Ni-Co-S-P	1 M KOH	280 mV	69 mV/dec	[52]
N,S-Co@C	1 M KOH	410 mV	101 mV/dec	[60]
Co_2NiO_x	1 M KOH	330 mV	54 mV/dec	[61]
Ru-CoNi@NC-2	1 M KOH	240 mV	75 mV/dec	[62]
IrO_2	1 M KOH	377 mV	171 mV/dec	[2]
Co_2NiP_x@C	1 M KOH	341 mV	73 mV/dec	This work
Co_2NiS_x@C	1 M KOH	332 mV	76 mV/dec	This work

The electrochemical stability of the material is obtained in two different ways. Figure 3.28 reveals that, after 1000 LSV cycles, the electrochemical performance of the Co_2NiP_X@C deteriorated slightly. The chronoamperometry and the polarization curve comparison method showed very similar results. Figure 3.32 shows that Co_2NiP_x@C still retained 70% of the current density after undergoing the 24 hour chronoamperometric testing.

Electrode conductivity is measured by the semicircle diameter of the fitted impedance spectrum of the electrochemical impedance. The smaller the resistance, the

better the electrode conductivity. The electrocatalytic activity of the material depends on the electrical conductivity of the material, the better the electrode conductivity, the faster the electron transfer, and the better the OER electrocatalytic performance. Figures 3.33-3.36 show the AC impedance spectra of $Co_2Ni(OH)_8$@C, Co_2NiO_4@C, Co_2NiS_X@C, and Co_2NiP_X@C at different voltages, respectively.

To compare the resistance and conductivity of these synthesized samples, the AC impedance spectra measured at 0.6 V for all samples were plotted in Figure 3.37, respectively. Both Co_2NiS_X@C, and Co_2NiP_X@C exhibit low internal resistance.

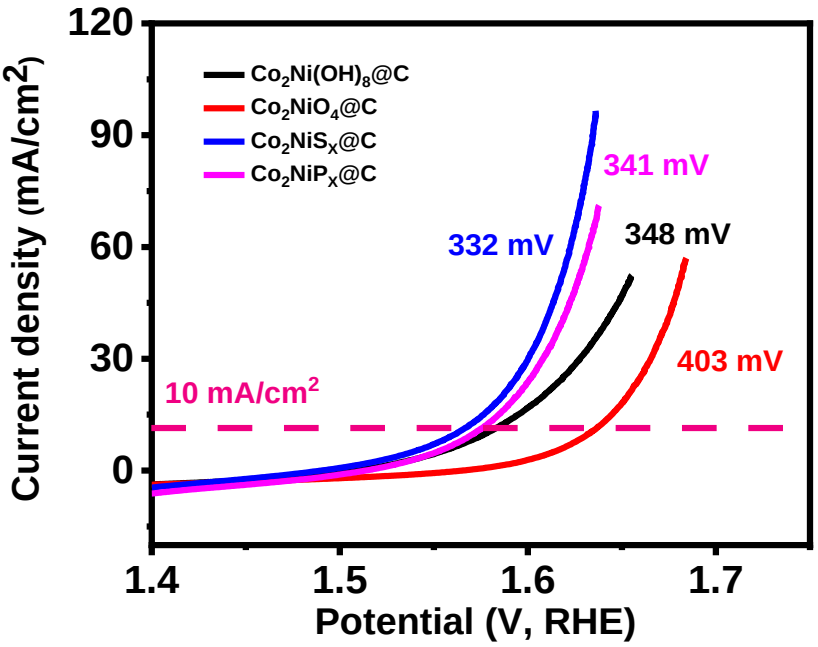

Figure 3.23. LSV-CV curves of $Co_2Ni(OH)_8$@C, Co_2NiO_4@C, Co_2NiS_X@C, and Co_2NiP_X@C for OER.

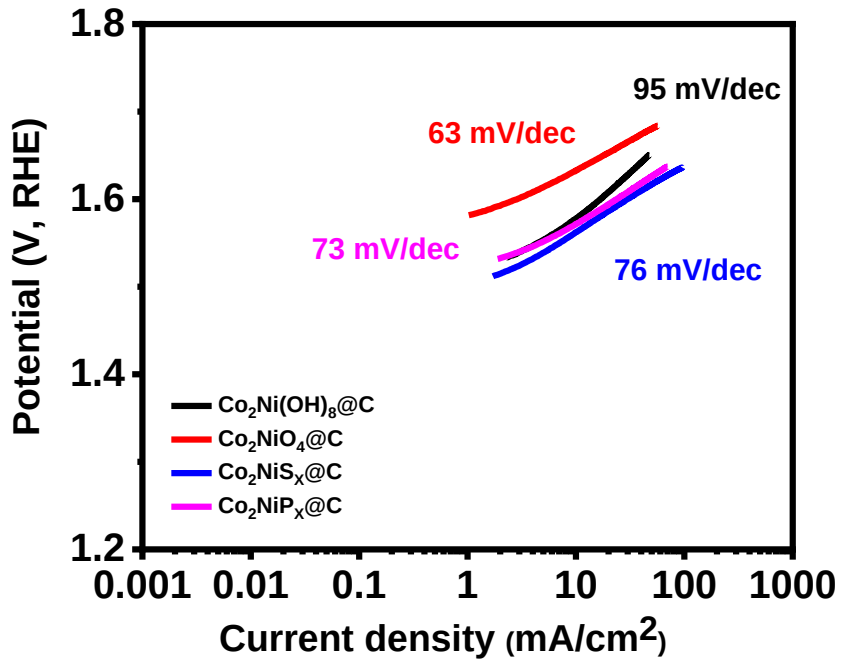

Figure 3.24. Tafel curves for $Co_2Ni(OH)_8$@C, Co_2NiO_4@C, Co_2NiS_X@C, and Co_2NiP_X@C.

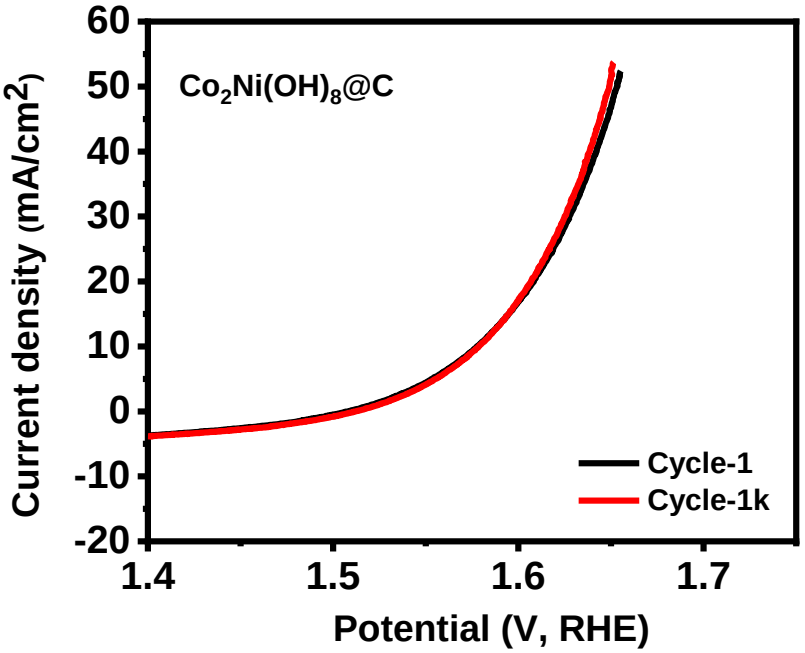

Figure 3.25. LSV-1 & LSV-1k OER stability test of $Co_2Ni(OH)_8$@C.

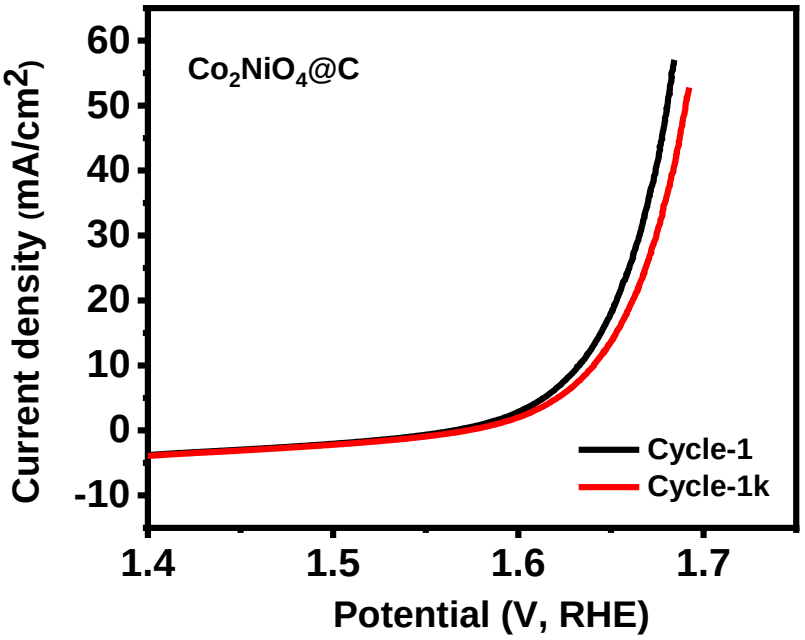

Figure 3.26. LSV-1 & LSV-1k OER stability test of Co_2NiO_4@C.

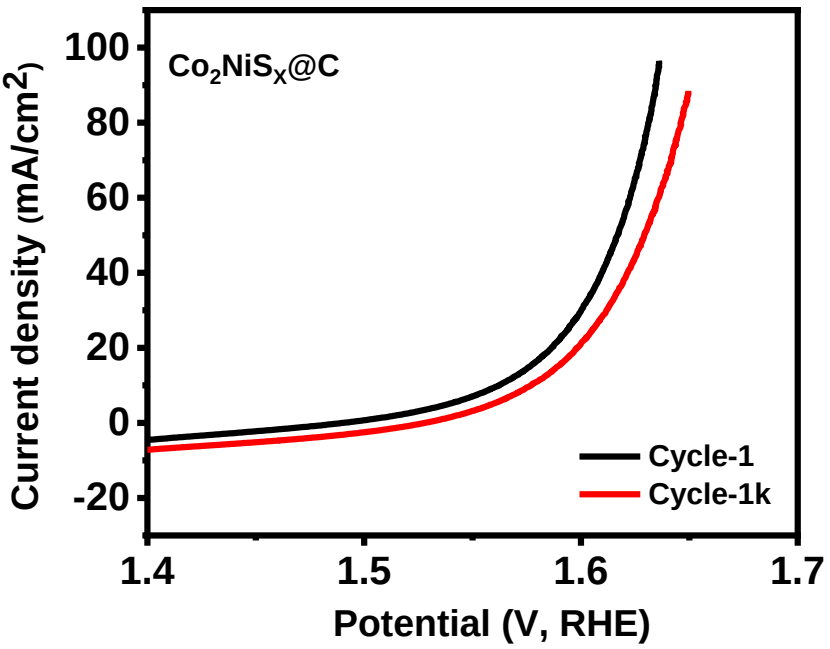

Figure 3.27. LSV-1 & LSV-1k OER stability test of Co_2NiS_X@C.

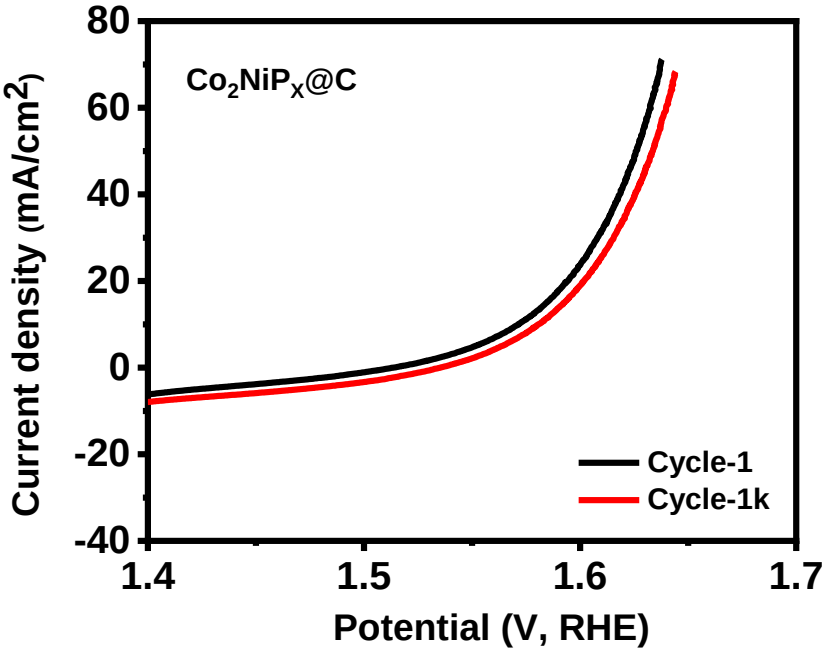

Figure 3.28. LSV-1 & LSV-1k OER stability test of Co_2NiP_X@C.

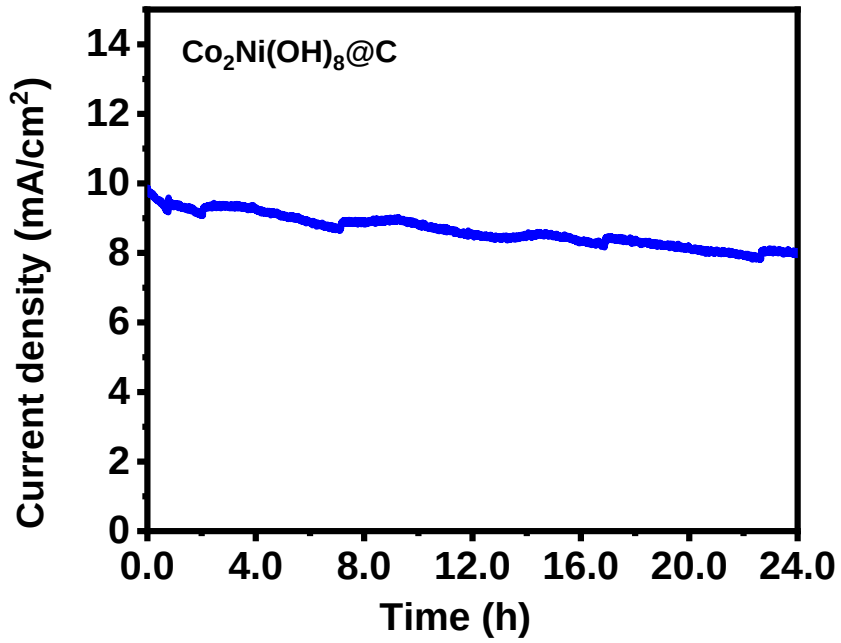

Figure 3.29. Chronoamperometry curve for $Co_2Ni(OH)_8$@C.

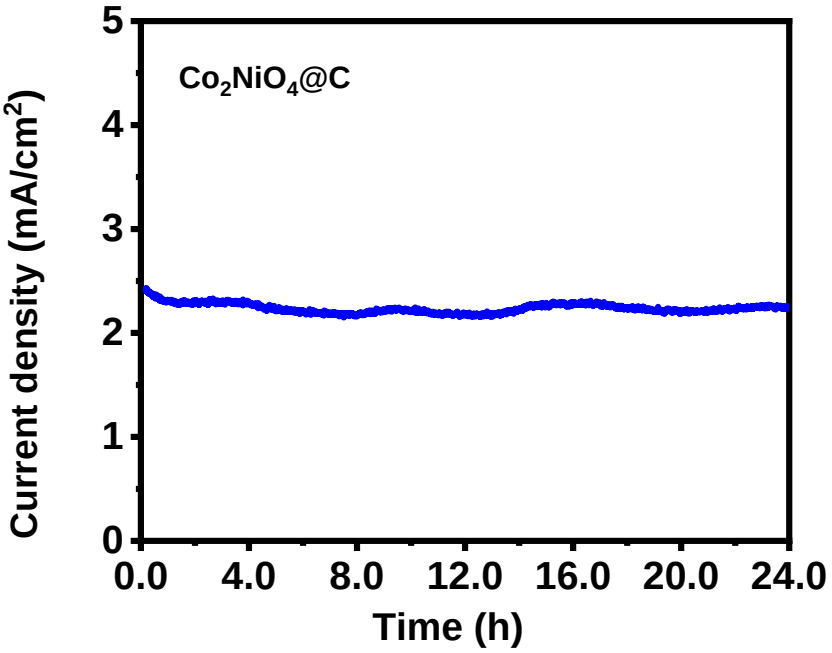

Figure 3.30. Chronoamperometry curve for Co_2NiO_4@C.

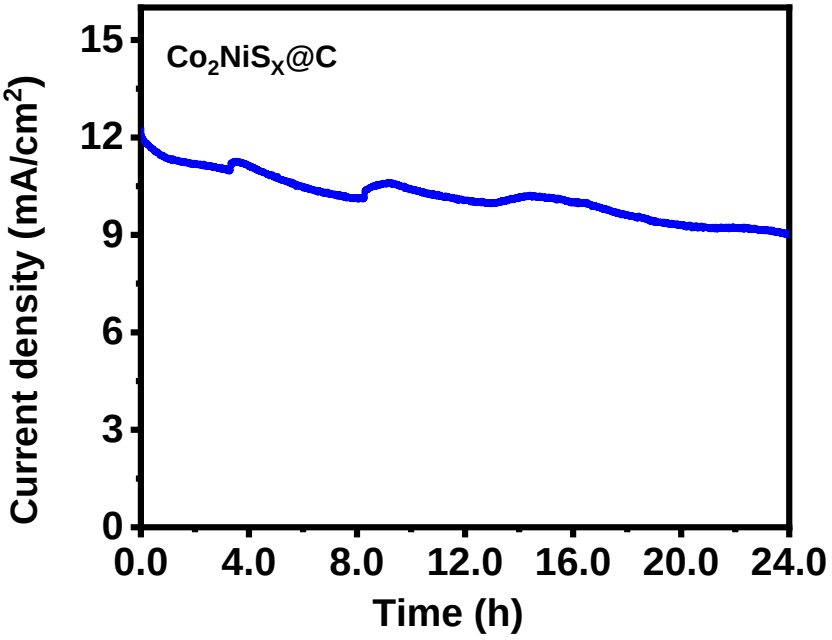

Figure 3.31. Chronoamperometry curve for Co_2NiS_X@C.

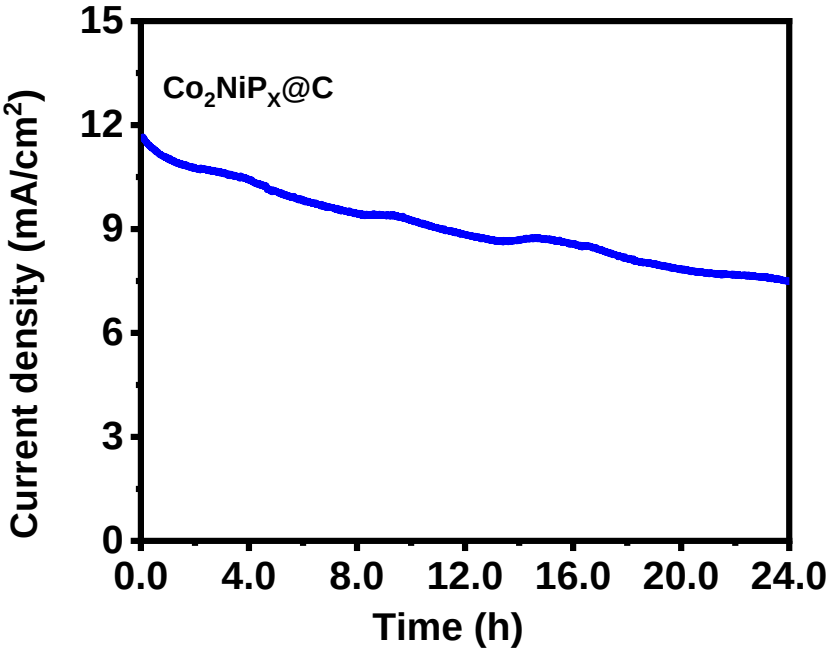

Figure 3.32. Chronoamperometry curve for Co_2NiP_X@C.

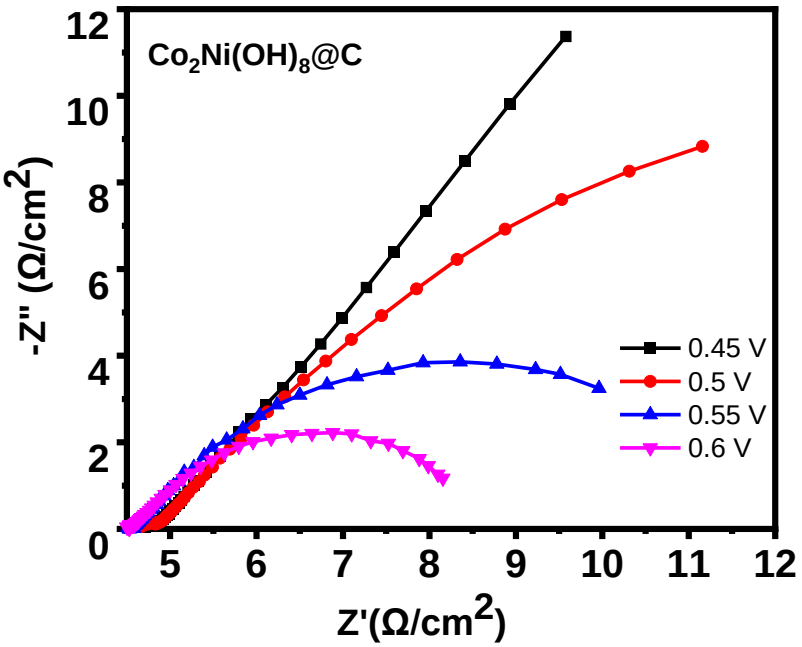

Figure 3.33. Nyquist plots for $Co_2Ni(OH)_8$@C at various applied potentials.

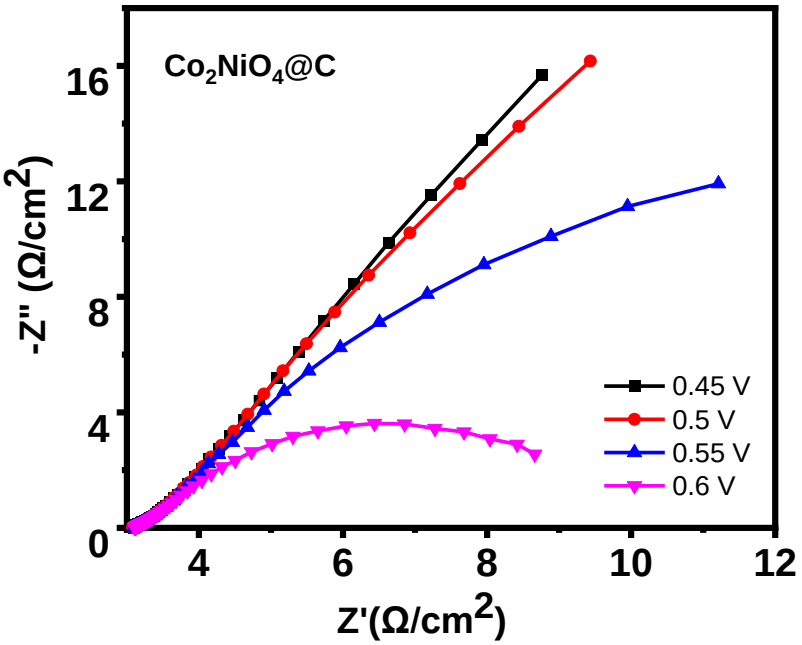

Figure 3.34. Nyquist plots for Co_2NiO_4@C at various applied potentials.

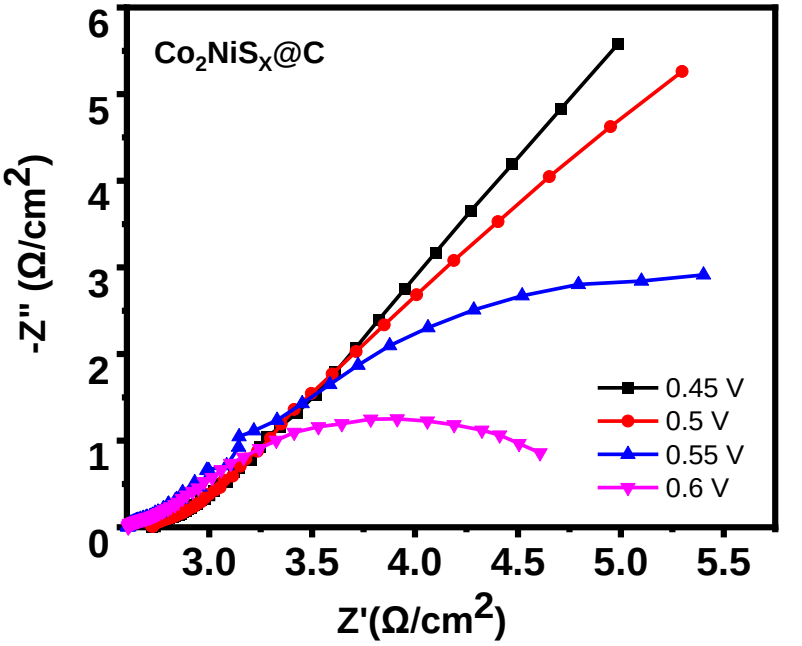

Figure 3.35. Nyquist plots for Co_2NiS_X@C at various applied potentials.

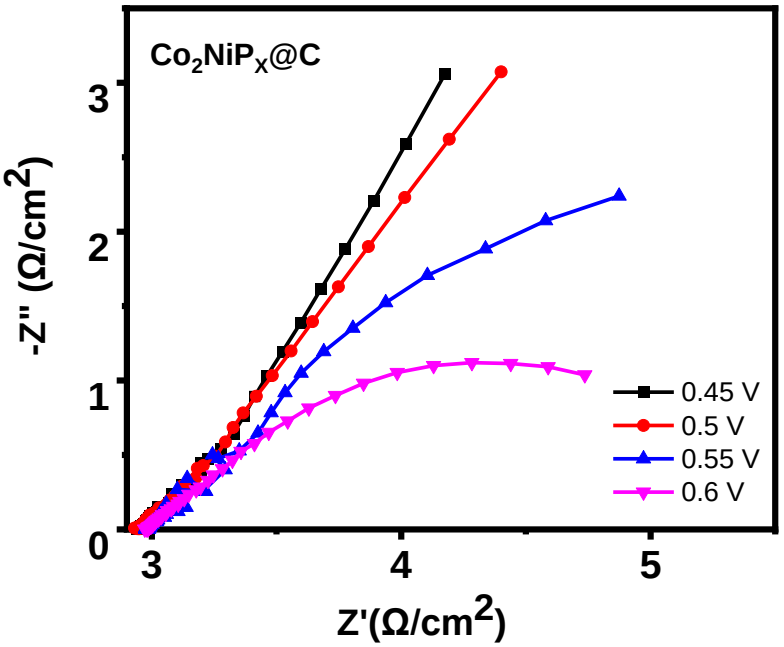

Figure 3.36. Nyquist plots for Co_2NiP_X@C at various applied potentials.

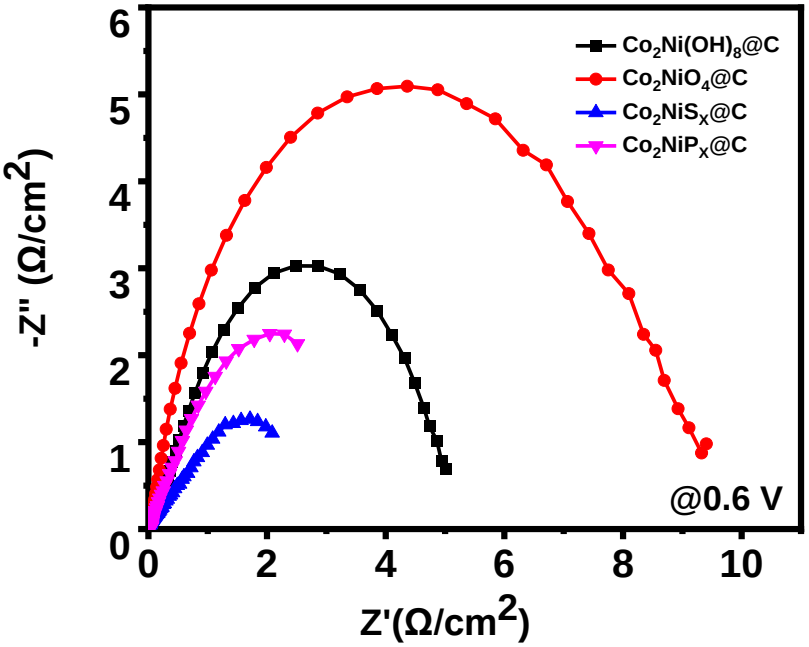

Figure 3.37. Nyquist plots for $Co_2Ni(OH)_8$@C, Co_2NiO_4@C, Co_2NiS_X@C, and Co_2NiP_X@C at 0.6 V.

3.2.1.3. Energy storage characteristic

Cobalt-nickel compounds are commonly used as energy storage materials for pseudocapacitors, and the energy storage properties of the synthesized materials have also been studied. First, all the materials were tested by cyclic voltammetry at different scan rates, from 300 mV/s to 2 mV/s in a 3M KOH solution, which are shown in figures 3.38-3.41. It can be seen that $Co_2Ni(OH)_8$@C, Co_2NiO_4@C, Co_2NiS_X@C, and Co_2NiP_X@C all exhibit typical pseudocapacitance characteristics due to the obvious redox peaks in their CV curves. When the scan rate was 300 mV/s, the current density flowing through Co_2NiP_x@C is much higher than other materials (Figure 3.42), which indicates that more energy can be stored by Co_2NiP_x@C than by the oxide or sulfide cobalt nickel compounds. Figure 3.43 shows the specific capacitance of various materials at different scan rates, that Co_2NiP_x@C exhibits the best capacitance characteristics of other synthesized materials, and its specific capacitance is as high as 16.7 F/cm^2 at a scan rate of 2mV/s.

Figures 3.44-3.47 show the discharge curves of $Co_2Ni(OH)_8$@C, Co_2NiO_4@C, Co_2NiS_X@C, and Co_2NiP_X@C at different discharge current densities, which can be confirmed that these materials have typical pseudocapacitive properties due to the reduction reaction in their discharge curves.

Figure 3.48 shows the specific capacitance of $Co_2Ni(OH)_8$@C, Co_2NiO_4@C, Co_2NiS_X@C, and Co_2NiP_X@C at different discharge current densities. Compared with $Co_2Ni(OH)_8$@C, the electrochemical performance of the material after sulfidation and phosphorizing treatment has been improved. In particular, the specific capacitance of

Co_2NiP_X@C was as high as 13.8 F/cm^2 when the GCD current density is 0.5 mA/cm^2. It is worth mentioning that Co_2NiP_X@C exhibits better rate performance than other synthesized materials, which is shown by the charge and discharge current density increased by 60 times from 0.5 mA/cm^2 to 30 mA/cm^2, the specific capacitance of the material was still as high as 7.2 F/cm^2. The Ragone plot (Figure 3.49) of the materials shows that Co_2NiP_X@C not only has a high-power density, but its energy density can also be as high as 6.4Wh/cm^2.

The stability curve of Co_2NiP_X@C is shown in Figure 3.50, which emphasizes the excellent electrochemical stability of the material. The specific capacitance retention rate of the material is as high as 90% after 5000 charge-discharge cycles. The Coulomb efficiency of a material refers to the ratio of the discharge capacity of the material to the charge capacity during the same cycle, which is nearly 100% during the entire charge and discharge process, emphasizing the high safety and stability of the material.

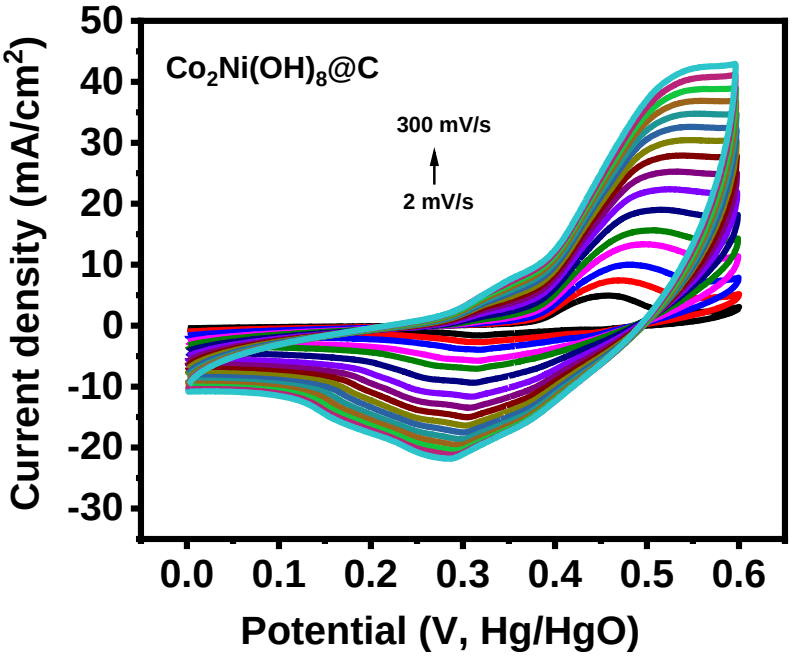

Figure 3.38. CV curves of $Co_2Ni(OH)_8$@C at different scan rates.

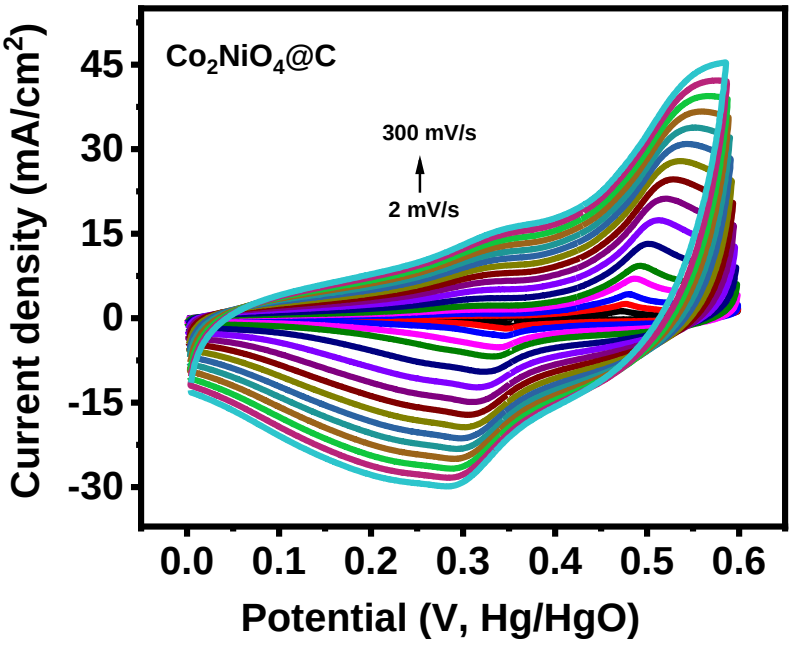

Figure 3.39. CV curves of Co_2NiO_4@C at different scan rates.

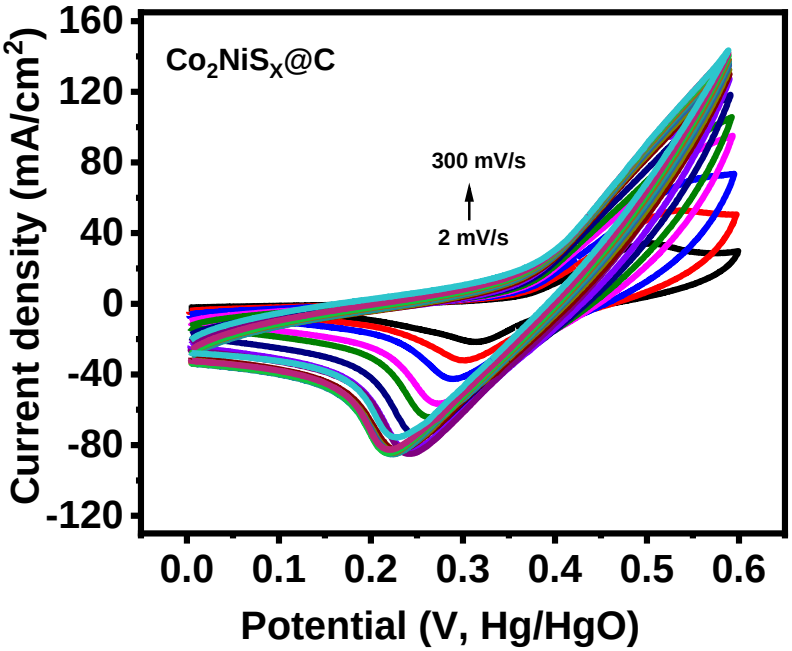

Figure 3.40. CV curves of Co_2NiS_X@C at different scan rates.

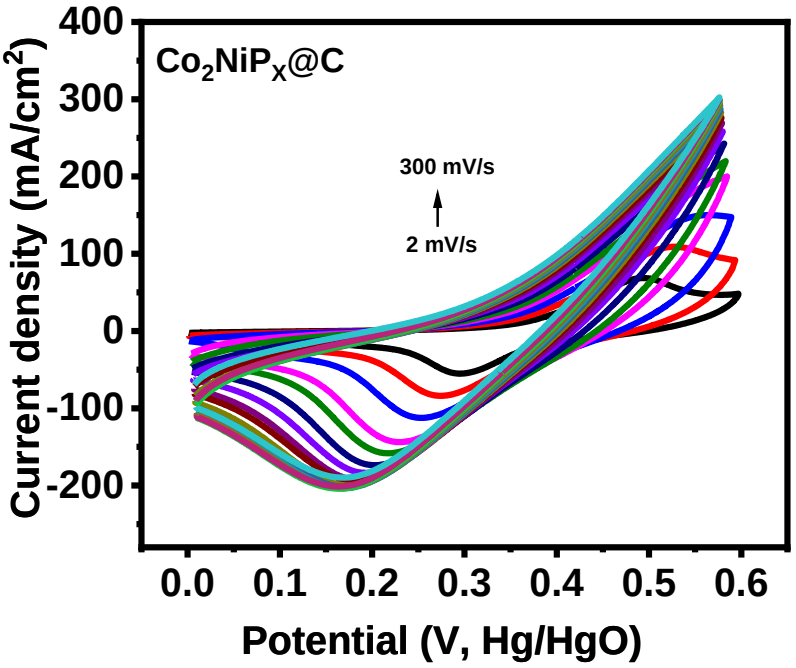

Figure 3.41. CV curves of Co_2NiP_X@C at different scan rates.

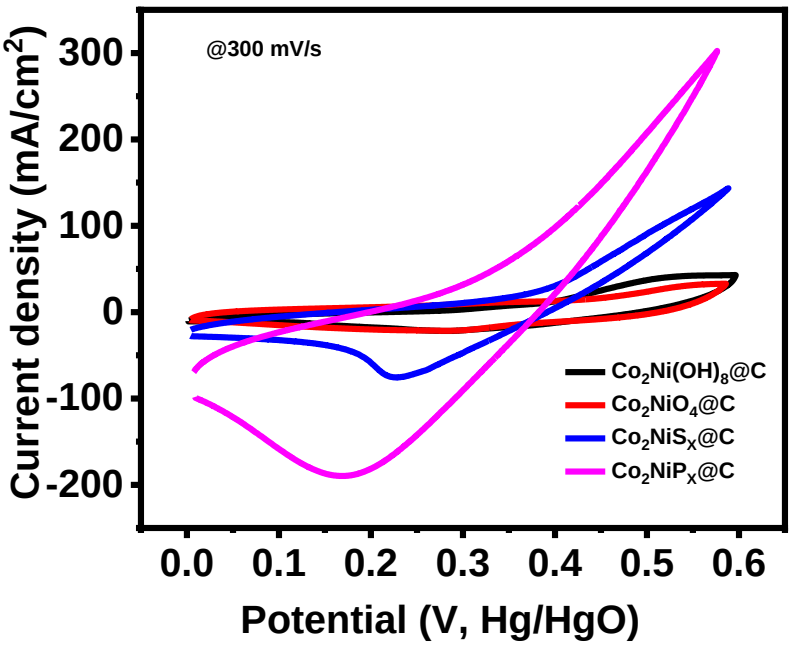

Figure 3.42. CV curves of $Co_2Ni(OH)_8$@C, Co_2NiO_4@C, Co_2NiS_X@C, and Co_2NiP_X@C at 300 mV.

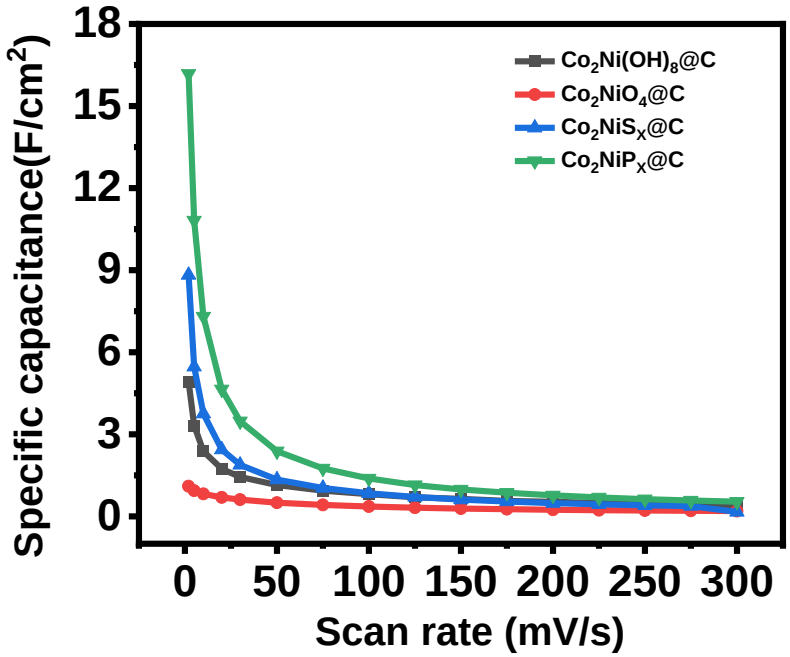

Figure 3.43. Specific capacitance versus scan rate for all the samples.

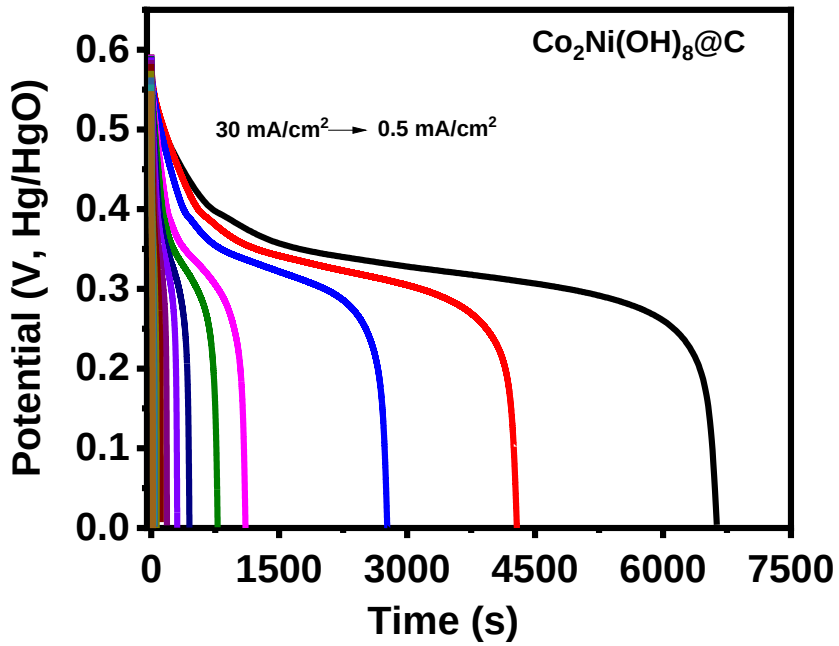

Figure 3.44. Potential versus time at different current density for $Co_2Ni(OH)_8$@C.

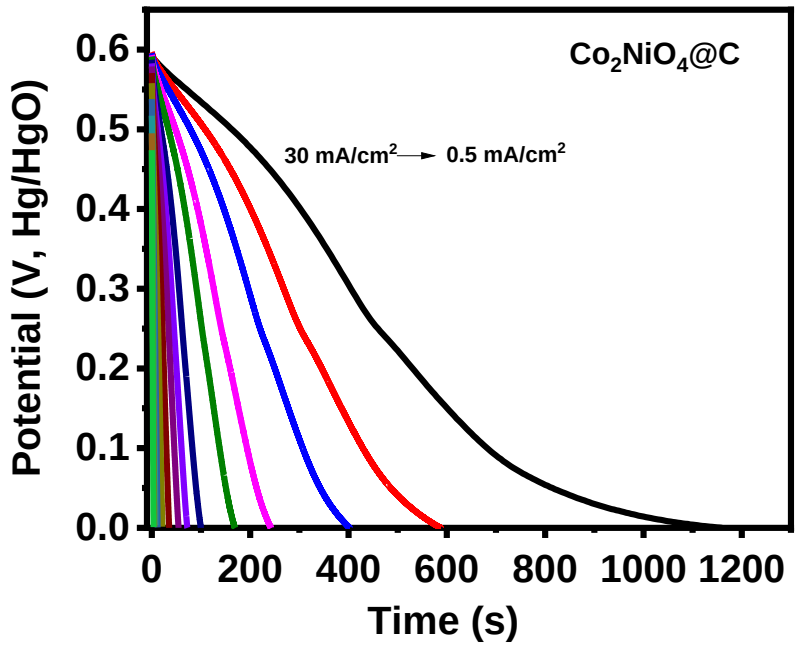

Figure 3.45. Potential versus time at different current density for Co_2NiO_4@C.

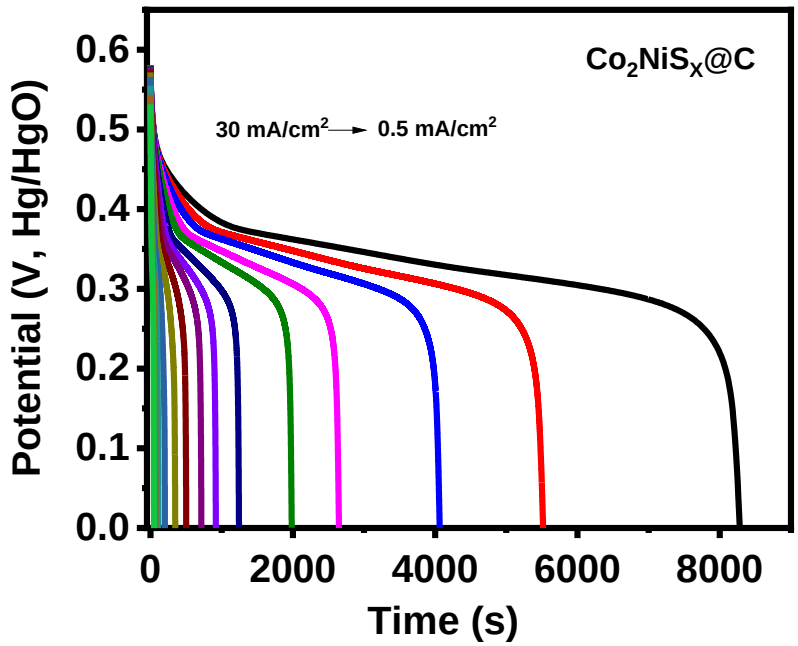

Figure 3.46. Potential versus time at different current density for Co_2NiS_X@C.

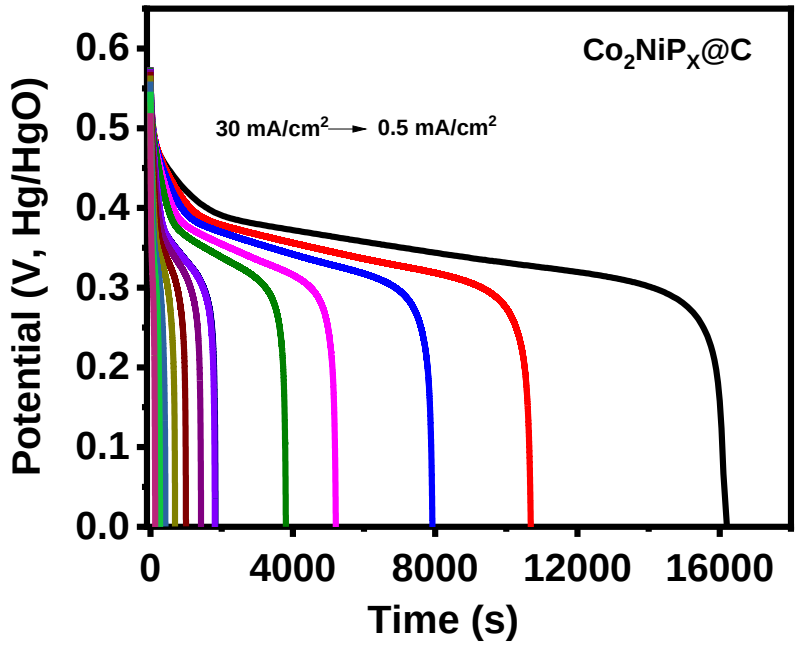

Figure 3.47. Potential versus time at different current density for Co_2NiP_X@C.

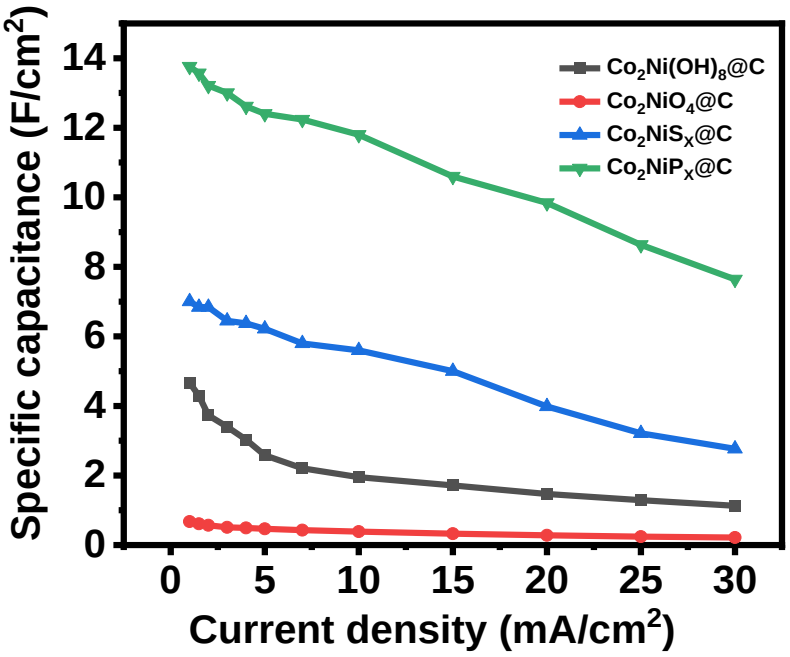

Figure 3.48. Specific capacitance versus current density for all the samples.

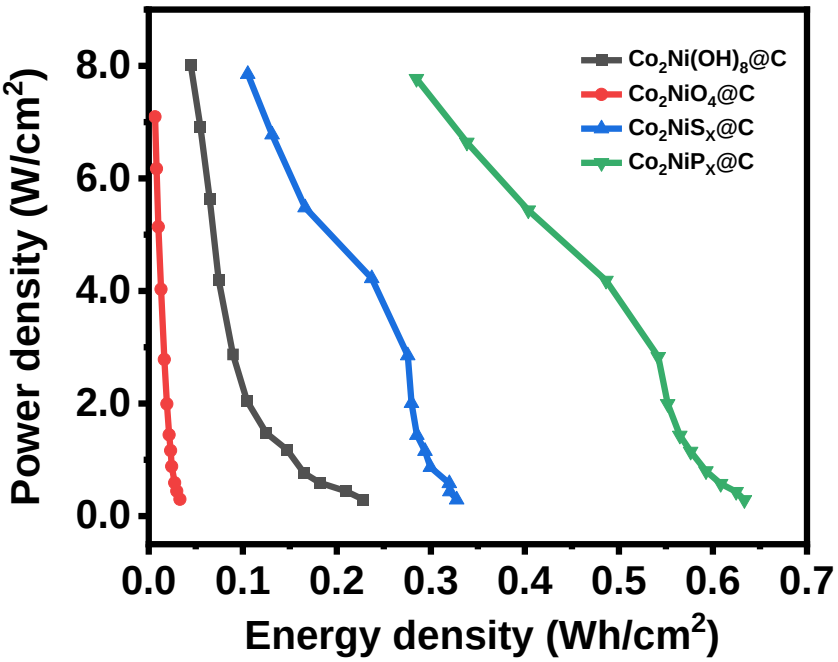

Figure 3.49. Power density versus energy density for all the samples.

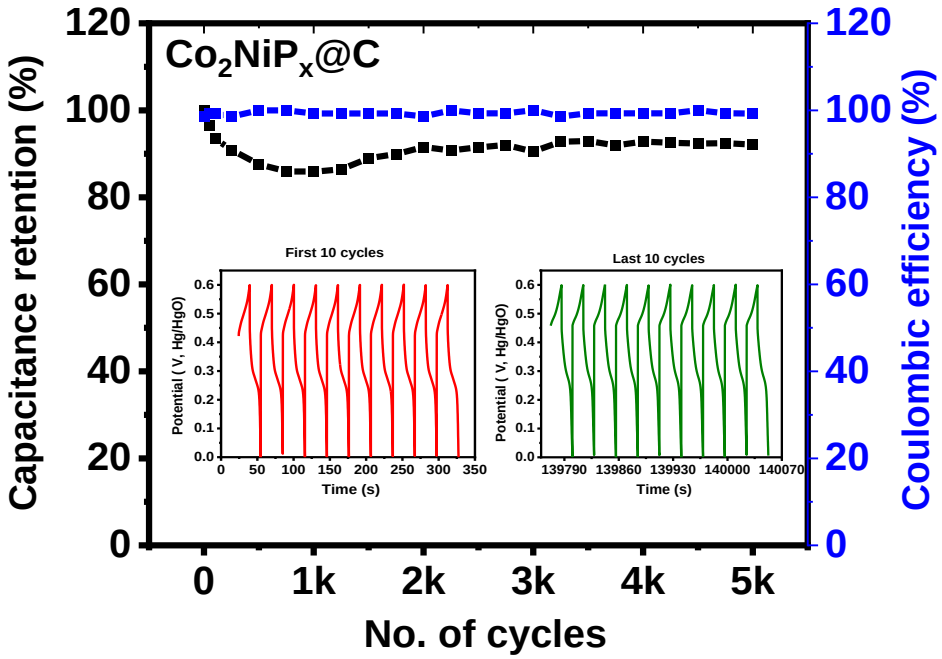

Figure 3.50. Stability curves for Co_2NiP_X@C.

Table 3. Comparison study of different Co-Ni electrode materials.

Similar work	Electrolyte	Specific capacitance	Current density	References
$CoNi_{300}/Cu_{120}$	1 M KOK	5743 mF/cm^2	1 mA/cm^2	[63]
CoMoO4@CoNiO2	2 M KOK	5.31 F/cm^2	5 mA/cm^2	[64]
$(CoxNi1-x)_9S_8$	1 M KOK	1.32 F/cm^2	1 mA/cm^2	[65]
$CoNi_2S_4$	3 M KOK	1722 F/g	1 A/g	[66]
CW@CoNiP-C	2 M KOK	2630 mF/cm^2	5 mA/cm^2	[67]
$Co_xNi_{1-x}P$/CNF	2 M KOK	3514 F/g	5 A/g	[68]
NiCo-MOF	2 M KOK	1202.1 F/g	1 A/g	[69]
$Co_{0.4}Ni_{0.6}(OH)_2$	6 M KOK	1843 F/g	0.5 A/g	[70]
Co–Ni–O/3DG	6 M KOK	1586 F/g	1 A/g	[71]
NiCo2O4	6 M KOK	2747.8 F/g	1 A/g	[72]
Co_2NiP_x@C	1 M KOK	13.8 F/cm^2	0.5 mA/cm^2	This work

In summary, nickel foam coated with activated carbon material was used as a precursor, and cobalt-nickel metallic nanomaterials were freely grown on its surface through the hydrothermal method. Then, the materials were calcined, sulfide, and phosphorized to explore the electrochemical performance of different cobalt-nickel metallic compounds. Co_2NiP_X@C attached to nickel foam shows outstanding performance in both HER and OER catalytic activity. For HER catalytic properties, Co_2NiP_X@C exhibits a low overpotential of 48 mV at 10 mA/cm^2. In addition, Co_2NiP_X@C also exhibits good electrochemical performance as an energy storage material for supercapacitors. The specific capacitance was as high as 13.8 F/cm^2 at 0.5 mA/cm^2 and the specific capacitance is still as high as 7.2 F/cm^2 at 30 mA/cm^2. Co_2NiP_X@C exhibits multifunctional electrochemical performance, outstanding OER catalytic activity, ultra-high specific capacitance and good rate capability. However, the synthesis process of these materials was complicated and lengthy. Therefore, in the second part of the work, our goal was to simplify the synthesis steps and shorten the synthesis time of these materials as much as possible on the premise of ensuring the original intention of the material design. In the second part of the work, commercial carbon as substrate instead of the previously synthesized carbon. The electrochemical synthesis method was used to replace the hydrothermal method.

3.2.2. Electrochemical characterization of Co-Ni compounds supported on carbon cloth

3.2.2.1. Hydrogen evolution reaction testing

The electrocatalytic and stability performances of the as-prepared materials were evaluated by the LSV-CV test in 1M KOH solution with a scan rate of 2mV/s. Figure 3.51 shows the LSV-CV polarization curves of all materials supported by carbon cloth, showing that $Co_2Ni(OH)_8$, Co_2NiO_4, Co_2NiS_X, and Co_2NiP_X exhibit the overpotential of 373, 332, 366, and 170 mV to reach a current density of 10 mA/cm^2, respectively. The corresponding Tafel slopes of these materials are shown in Figure 3.52, $Co_2Ni(OH)_8$, Co_2NiO_4, and Co_2NiS_X exhibit high Tafel Slope of 320, 206, and 391 mV/dec, respectively. Co_2NiP_X has a lower Tafel slope of 143 mV/dec in comparison, emphasizing that it is less kinetic barrier in the HER reaction. The electrochemical stability of these synthesized cobalt-nickel compounds on carbon cloth were obtained by comparing their initial LSV-CV polarization curves with the 1000^{th} cycle LSV-CV polarization curves. Figures 3.53-3.56 show the initial LSV-CV and the 1000^{th} LSV-CV curves of $Co_2Ni(OH)_8$, Co_2NiO_4, Co_2NiS_X, and Co_2NiP_X, respectively. All these materials exhibit relatively stable HER electrocatalytic stability since their initial LSV-CV polarization curves and the 1000^{th} LSV-CV polarization curves overlap with each other.

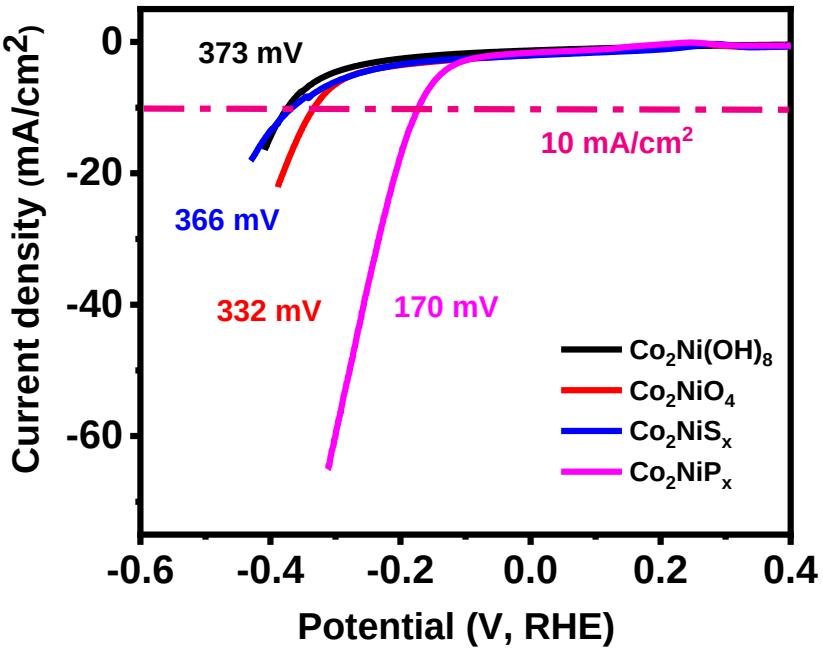

Figure 3.51. LSV-CV curves of $Co_2Ni(OH)_8$, Co_2NiO_4, Co_2NiS_X, and Co_2NiP_X for HER.

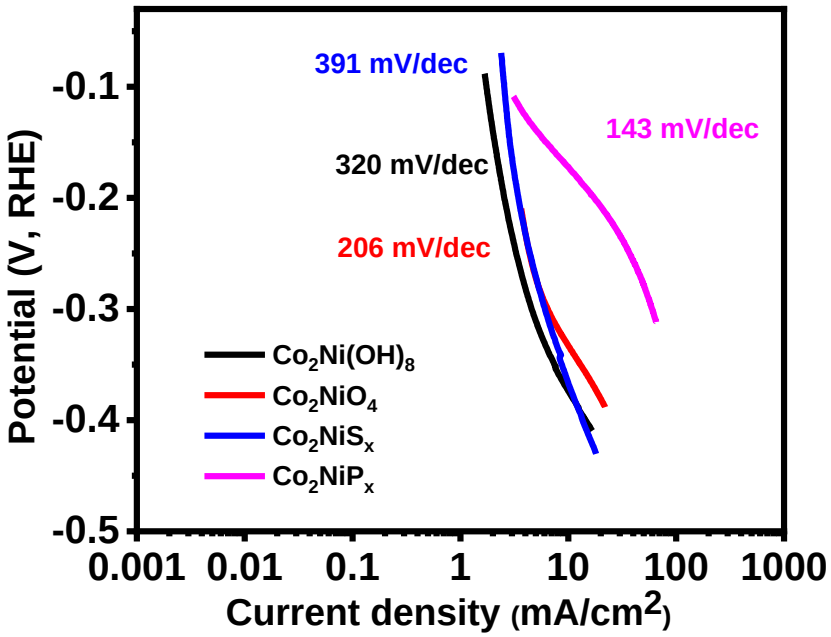

Figure 3.52. Corresponding Tafel curves for $Co_2Ni(OH)_8$, Co_2NiO_4, Co_2NiS_X, and Co_2NiP_X.

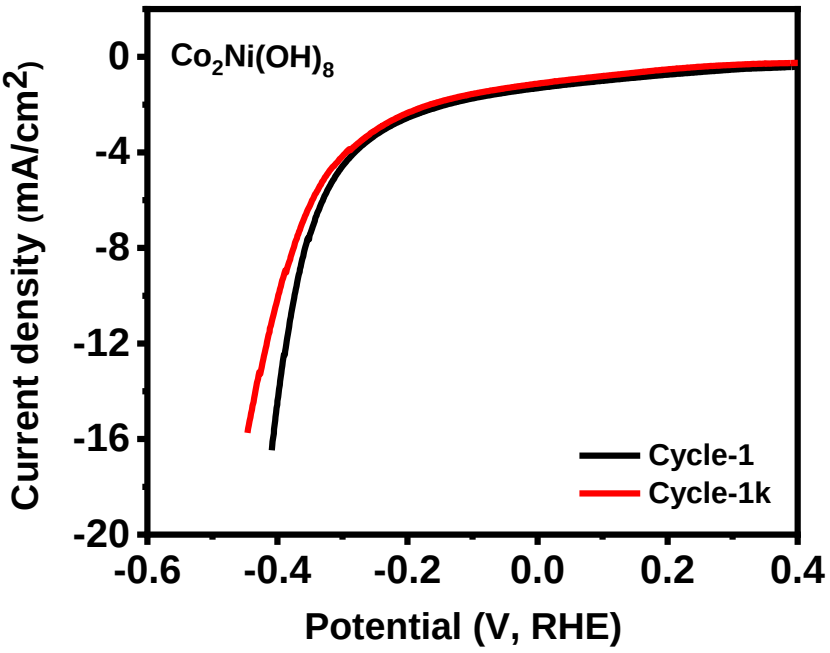

Figure 3.53. LSV-1 & LSV-1k HER stability test of the $Co_2Ni(OH)_8$.

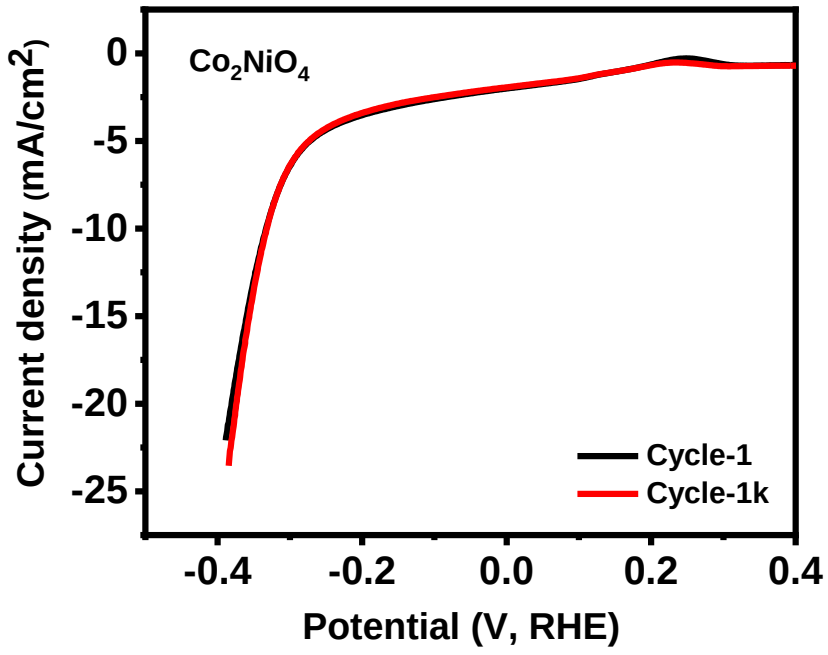

Figure 3.54. LSV-1 & LSV-1k HER stability test of the Co_2NiO_4.

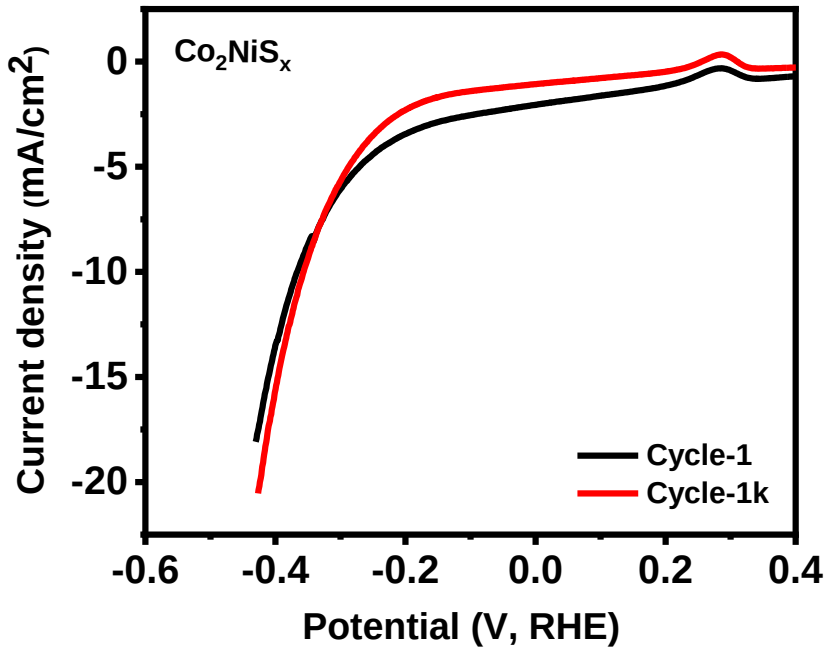

Figure 3.55. LSV-1 & LSV-1k HER stability test of the Co_2NiS_X.

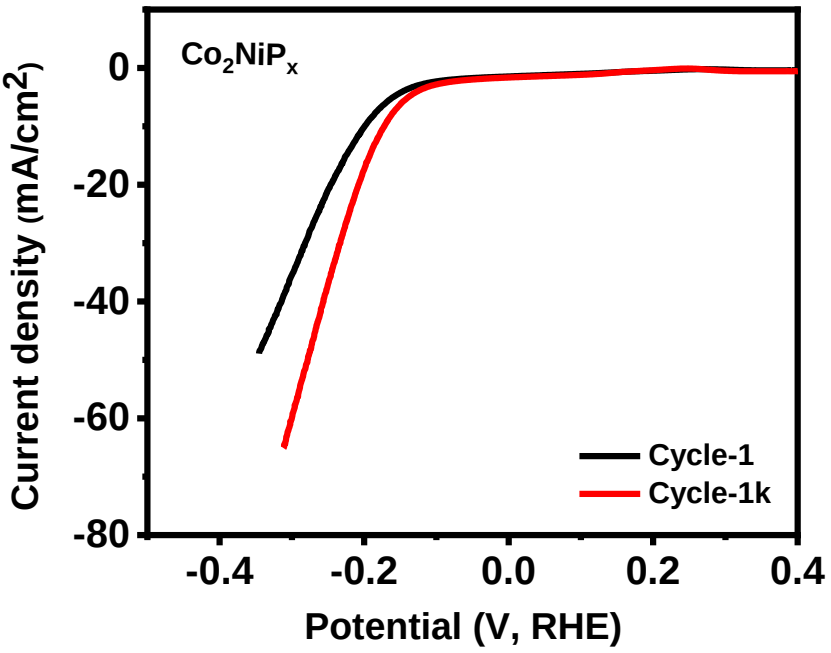

Figure 3.56. LSV-1 & LSV-1k HER stability test of the Co_2NiP_X.

3.2.2.2. Oxygen evolution reaction testing

The electrocatalytic properties of these materials were studied through a three-electrode system as oxygen evolution catalysts. Linear sweep voltammetry and cyclic voltammetry (LSV-CV) tests were performed to explore the overpotential and Tafel slope of these materials under OER conditions. Figures 3.57 and 3.58 show the LSV-CV polarization curves and Tafel slopes of $Co_2Ni(OH)_8$, Co_2NiO_4, Co_2NiS_X, and Co_2NiP_X, respectively. $Co_2Ni(OH)_8$, Co_2NiO_4, Co_2NiS_X, and Co_2NiP_X show overpotentials of 350, 370, 280, and 330 mV correspond to Tafel slopes of 64, 72, 77, and 60 mV/dec. The OER electrochemical stability of these materials is shown by chronoamperometry and polarization curve comparison, respectively in Figure. 3.59-3.66. From the comparison of the initial LSV polarization curves of these materials with the LSV curves of the 1000 cycles, their electrochemical stability are good because their LSV-1 and LSV-1k coincide with each other. Furthermore, chronopotentiometry was used to reveal the electrochemical stability of these electrochemically synthesized materials under OER conditions. The current densities flowing through $Co_2Ni(OH)_8$, Co_2NiO_4, Co_2NiS_X, and Co_2NiP_X decrease to 68%, 55%, 62% and 59%, respectively after 24 hours. Electrochemical Impedance Spectroscopy was also performed under OER conditions to study the electrical conductivity of these materials. The results are shown in Figures 3.67-3.70, that the phosphorized and sulfurized samples have small internal resistance.

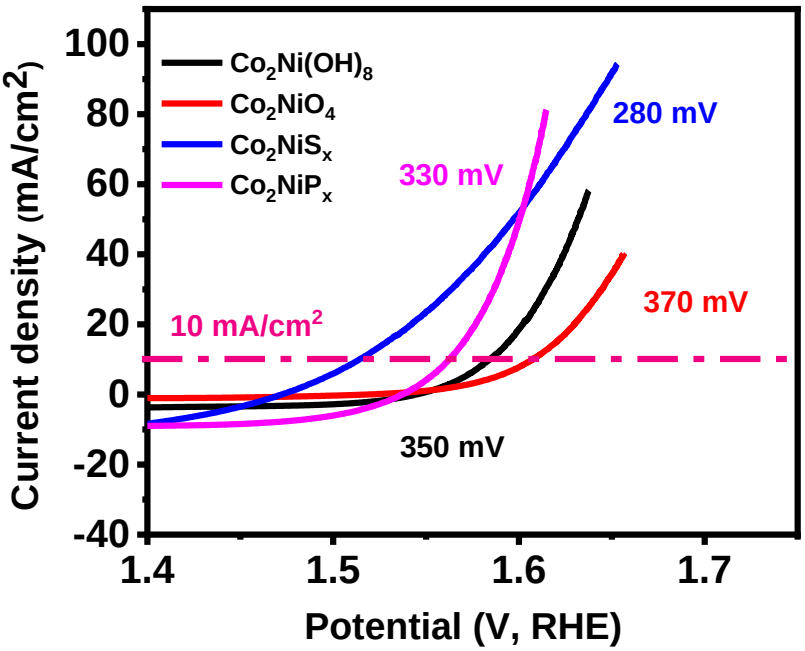

Figure 3.57. LSV-CV curves of $Co_2Ni(OH)_8$, Co_2NiO_4, Co_2NiS_X, and Co_2NiP_X for OER.

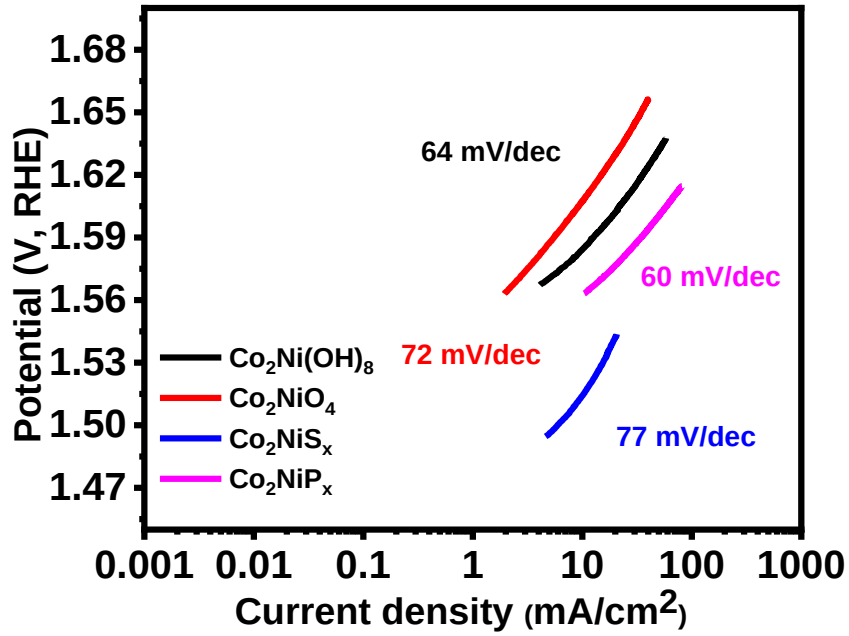

Figure 3.58. Corresponding Tafel curves for $Co_2Ni(OH)_8$, Co_2NiO_4, Co_2NiS_X, and Co_2NiP_X.

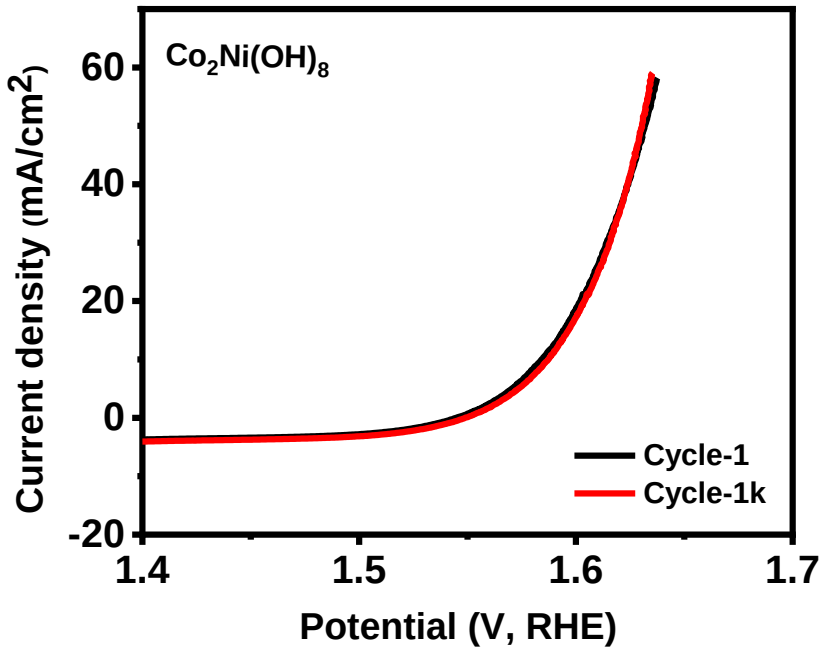

Figure 3.59. LSV & LSV-1k OER stability test of $Co_2Ni(OH)_8$.

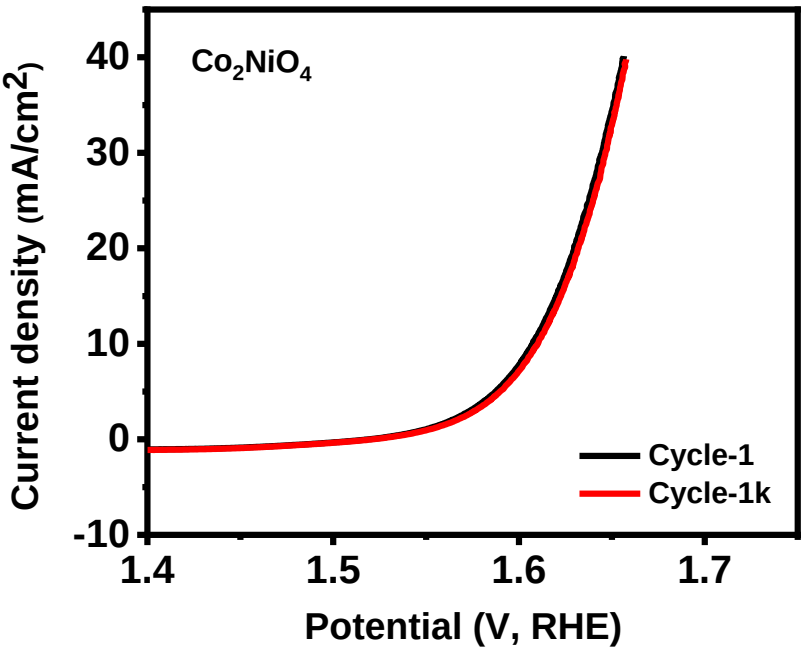

Figure 3.60. LSV & LSV-1k OER stability test of Co_2NiO_4.

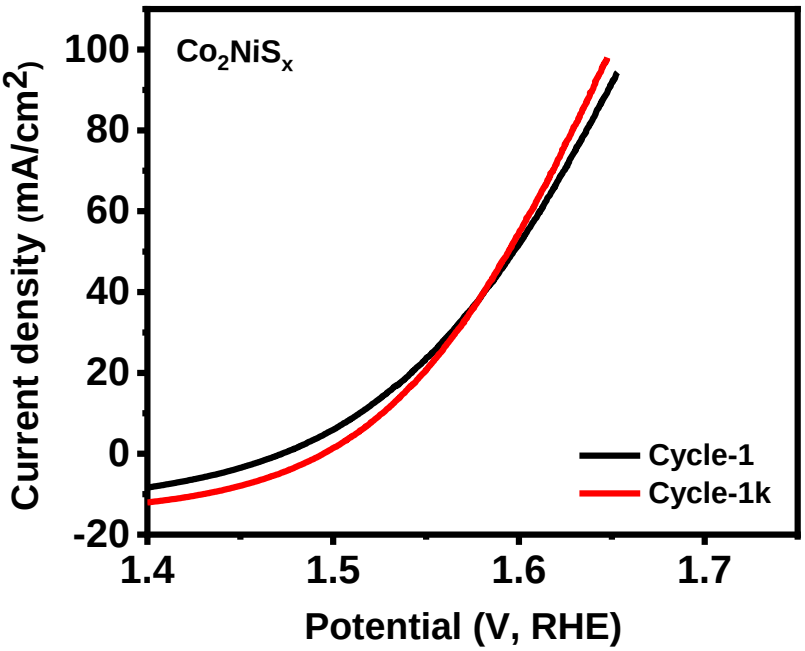

Figure 3.61. LSV & LSV-1k OER stability test of Co_2NiS_X.

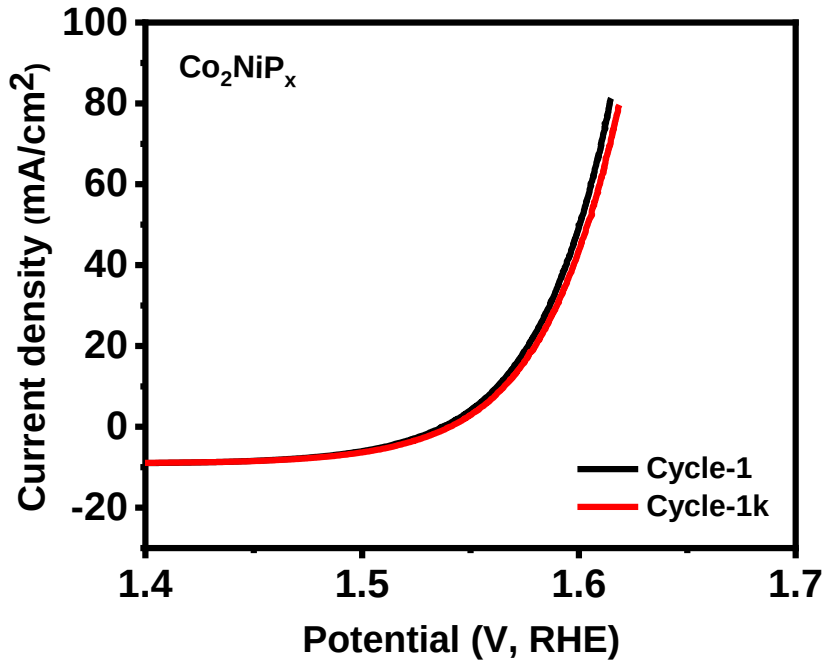

Figure 3.62. LSV & LSV-1k OER stability test of Co_2NiP_X.

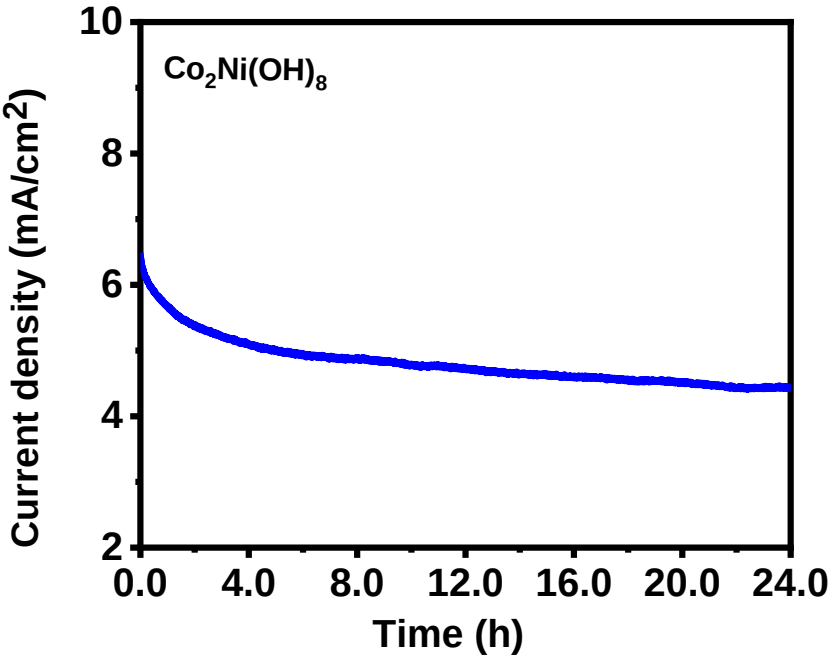

Figure 3.63. Chronoamperometry curve for $Co_2Ni(OH)_8$.

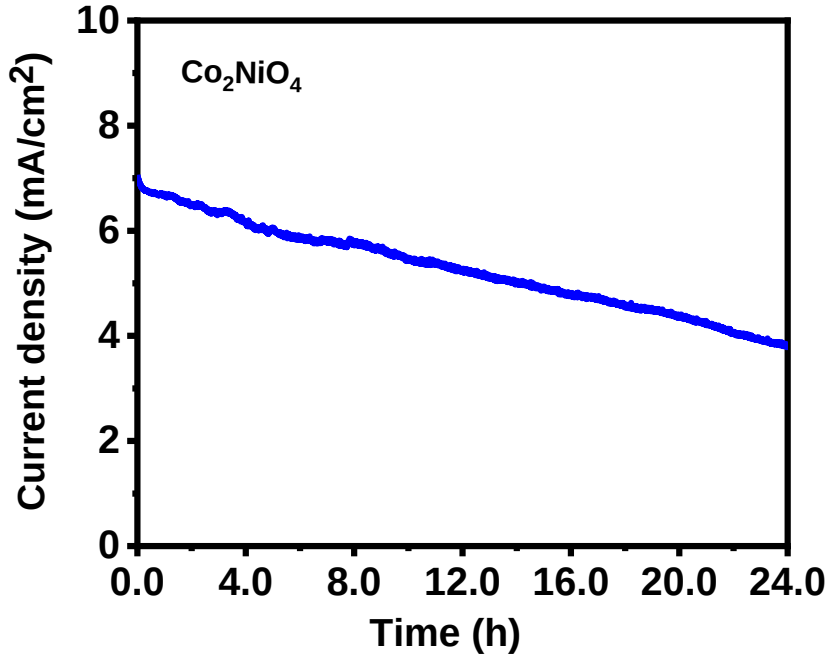

Figure 3.64. Chronoamperometry curve for Co_2NiO_4.

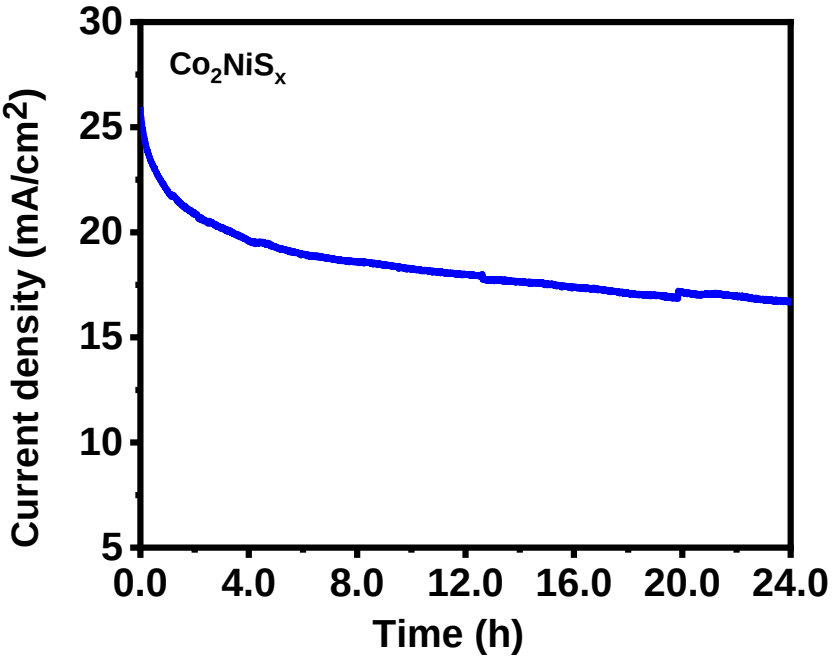

Figure 3.65. Chronoamperometry curve for Co_2NiS_X.

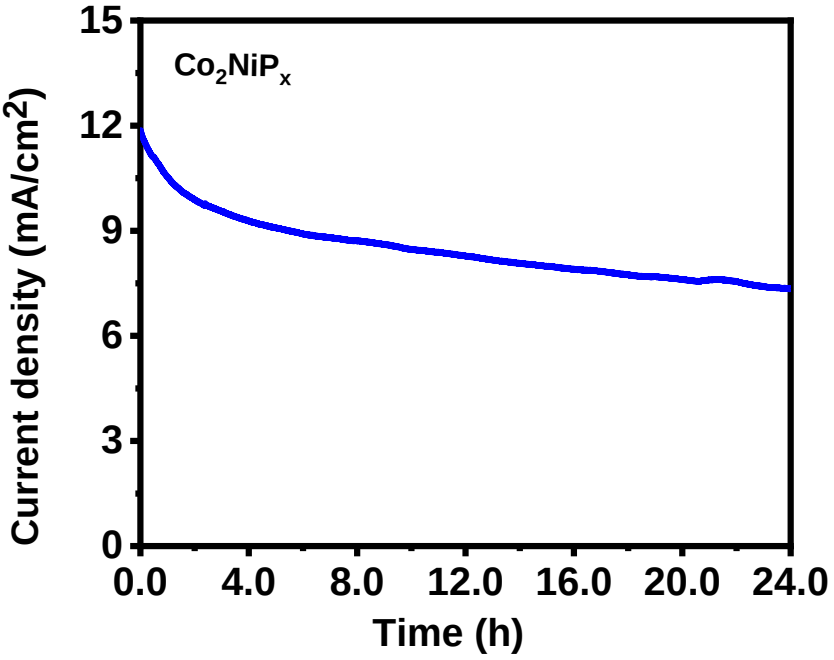

Figure 3.66. Chronoamperometry curve for Co_2NiP_X.

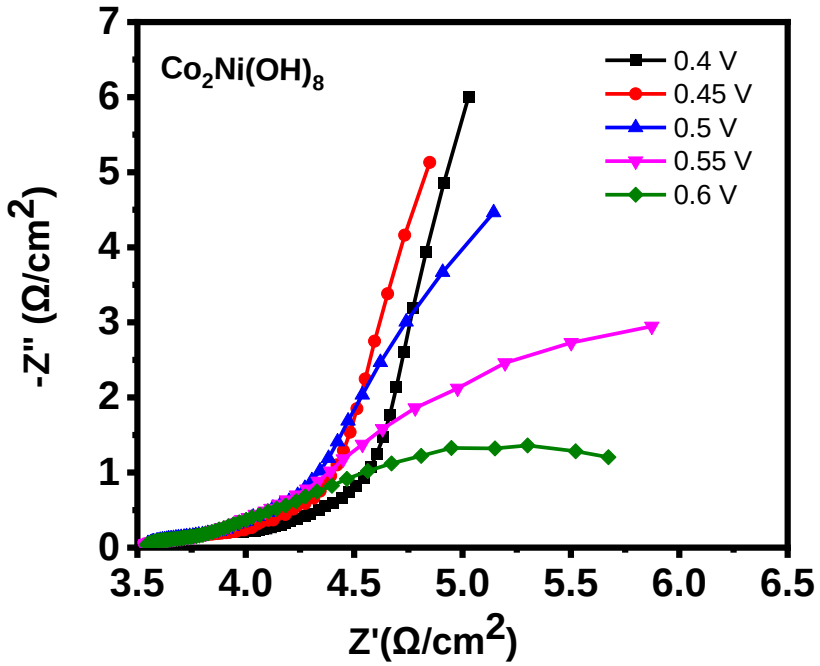

Figure 3.67. Nyquist plots for $Co_2Ni(OH)_8$ at various applied potentials.

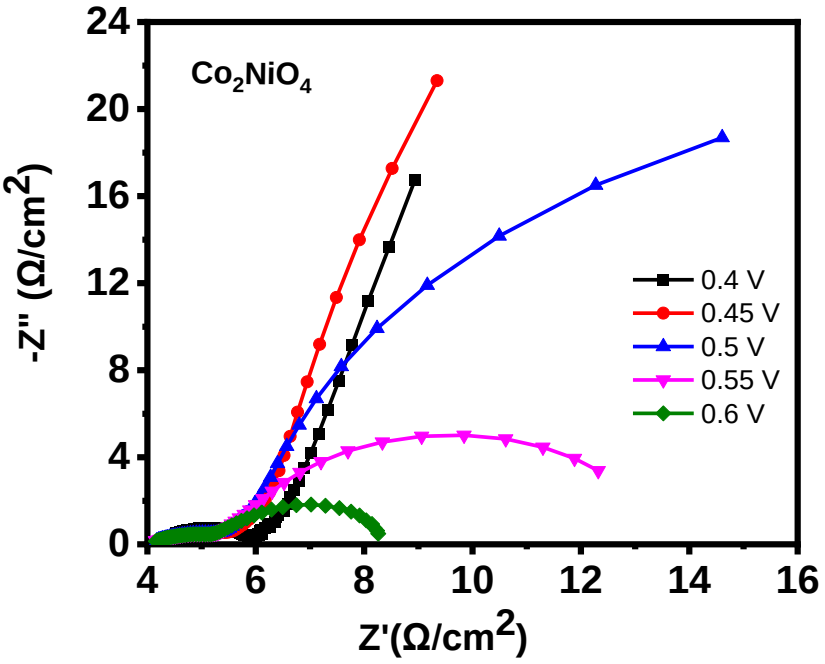

Figure 3.68. Nyquist plots for Co_2NiO_4 at various applied potentials.

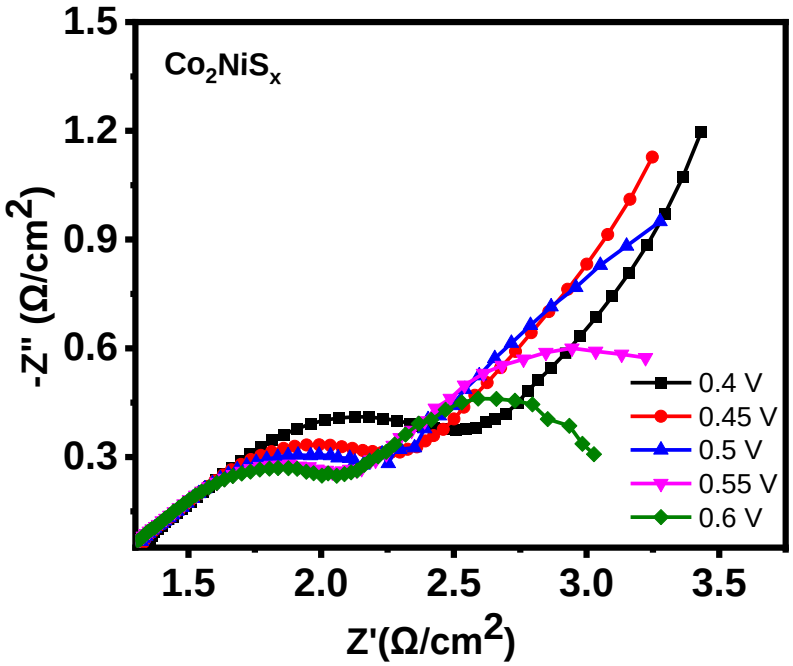

Figure 3.69. Nyquist plots for Co_2NiS_X at various applied potentials.

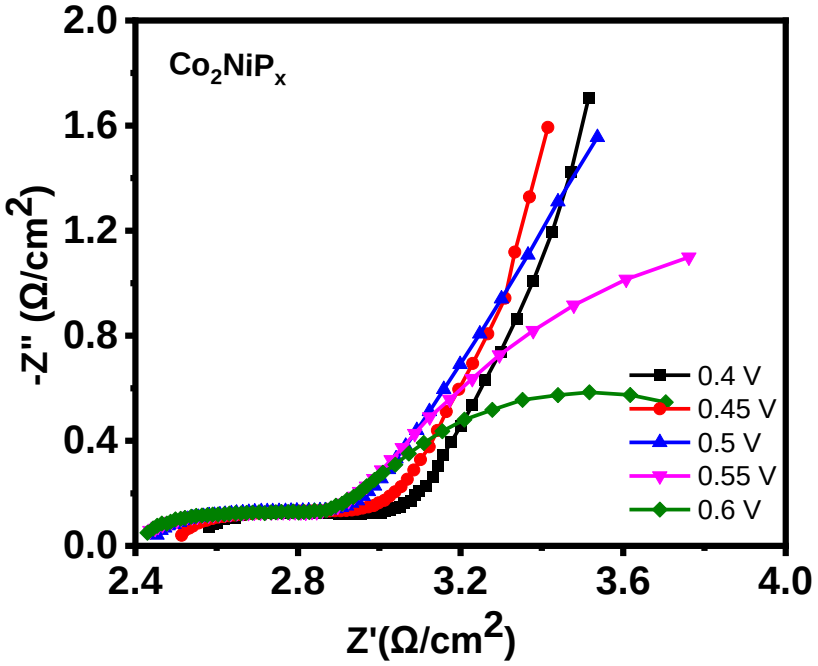

Figure 3.70. Nyquist plots for Co_2NiP_X at various applied potentials.

3.2.2.3. Energy storage characteristic

Cobalt-nickel compounds supported by carbon cloth were also studied for energy storage performance. First, these materials were tested by CV at different scan rates, from 300 mV/s to 2 mV/s between 0-0.6 V. The CV curves of $Co_2Ni(OH)_8$, Co_2NiO_4, Co_2NiS_X, and Co_2NiP_X are shown in Figures 3.71-3.74, emphasize the typical pseudocapacitive properties and good electrochemical reversibility of these synthesized materials. To obtain information on the specific capacitance, power density, and energy density of these materials, GCD tests were performed. Figures 3.75-3.78 show the result curves of GCD at different current densities, emphasizing the pseudocapacitive properties of these materials. The specific capacitances of $Co_2Ni(OH)_8$, Co_2NiO_4, Co_2NiS_X, and Co_2NiP_X were calculated and plotted in Figure 3.79 Co_2NiP_X exhibits excellent electrochemical properties as an energy storage material for supercapacitors compared to $Co_2Ni(OH)_8$, Co_2NiO_4, Co_2NiS_X. Specifically reflected in: ultra-high specific capacitance, 9.8 F/cm^2 at 1 A/cm^2. Good rate performance, when the charge and discharge current density is increased thirty times from 1 A/cm^2 to 30 A/cm^2, the specific capacitance retention is as high as 86%. Figure 3.80 shows the Ragon diagrams of $Co_2Ni(OH)_8$, Co_2NiO_4, Co_2NiS_X, and Co_2NiP_X, respectively. Co_2NiP_X exhibits a high energy density as high as 0.42 Wh/cm^2.

The stability curve for Co_2NiP_X@C is shown in Figure 3.81, which demonstrates the electrochemical stability of the material. The specific capacitance retention rate of the material is 50% after 5000 charge-discharge cycles. The Coulombic efficiency of a material refers to the ratio of the discharge capacity of the material to the charge capacity during

the same cycle, which is nearly 100% during the entire charge and discharge process, emphasizing the high safety and stability of the material.

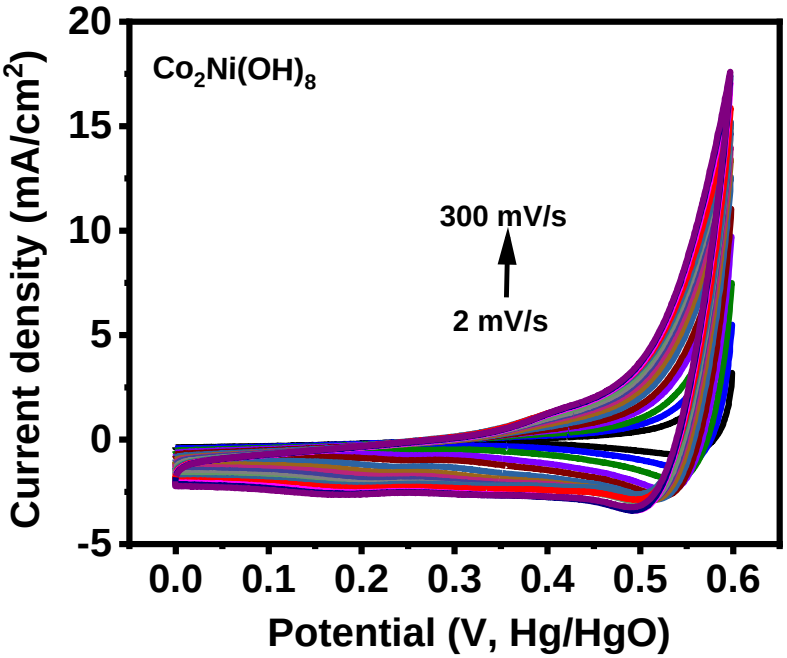

Figure 3.71. CV curves of $Co_2Ni(OH)_8$ at different scan rates.

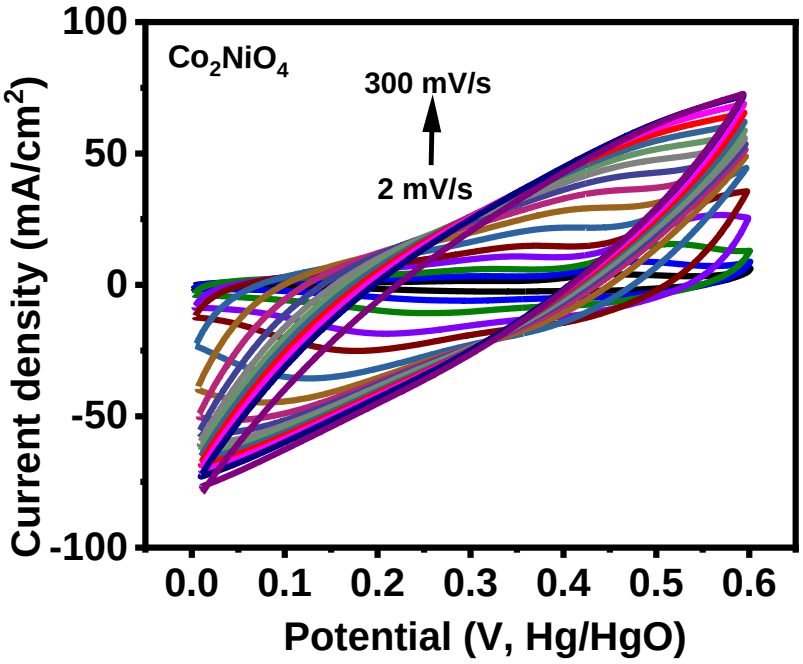

Figure 3.72. CV curves of Co_2NiO_4 at different scan rates.

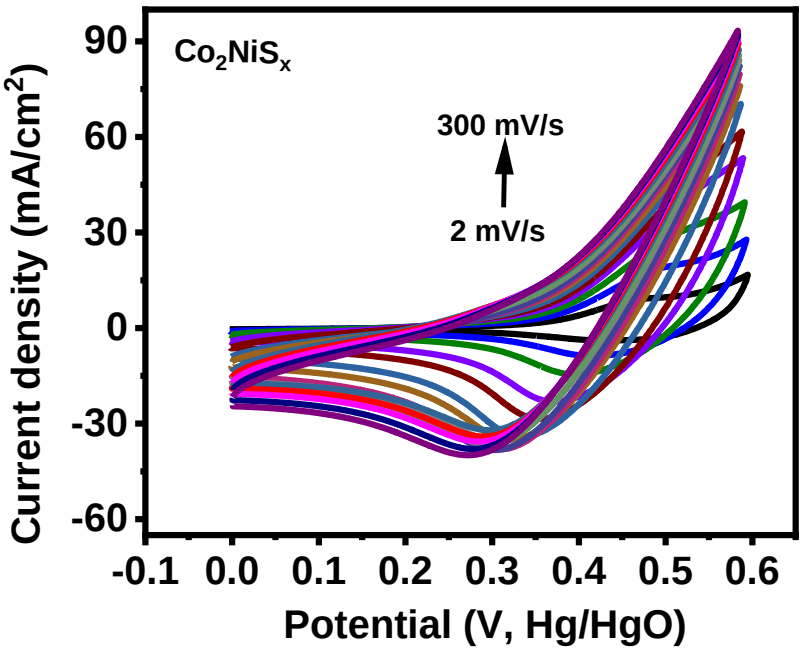

Figure 3.73. CV curves of Co_2NiS_X at different scan rates.

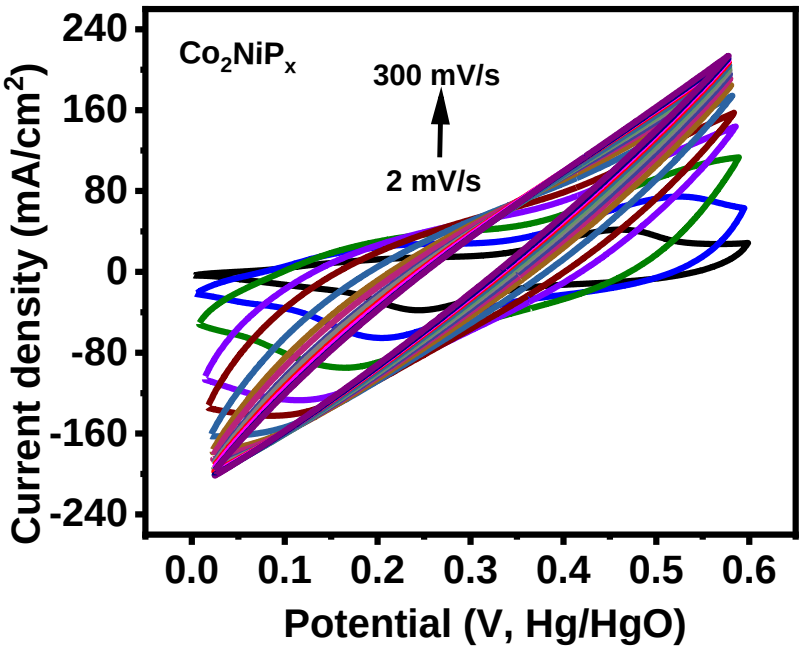

Figure 3.74. CV curves of Co_2NiP_X at different scan rates.

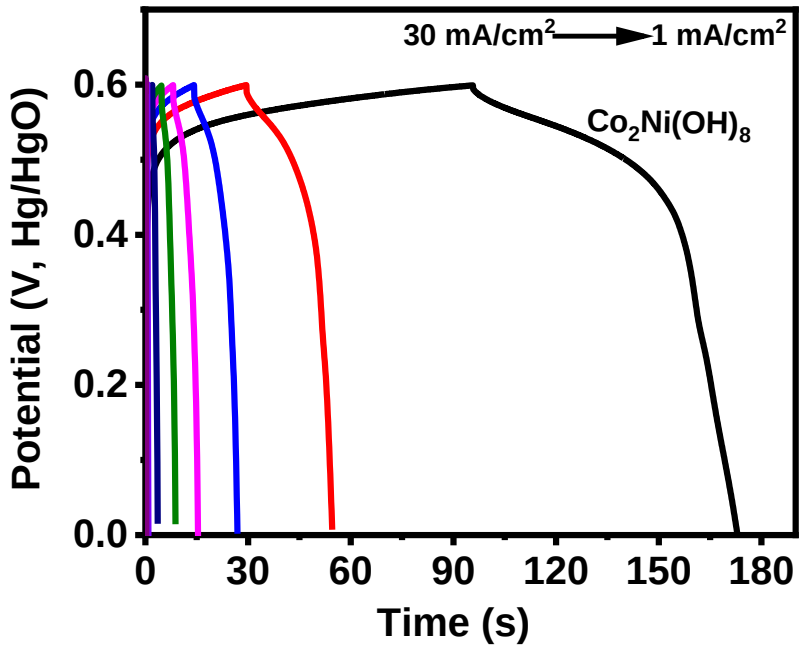

Figure 3.75. Potential versus time at different current density for $Co_2Ni(OH)_8$.

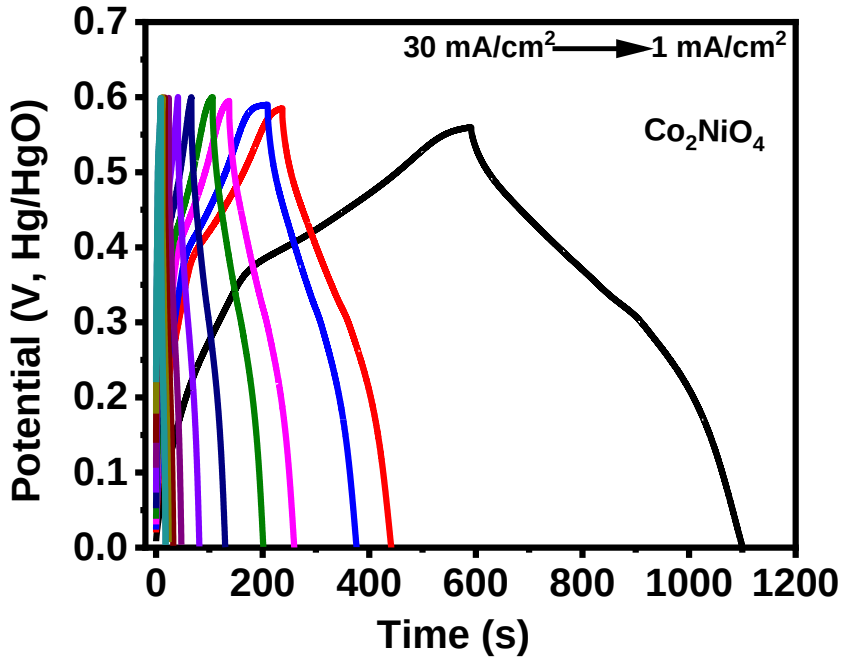

Figure 3.76. Potential versus time at different current density for Co_2NiO_4.

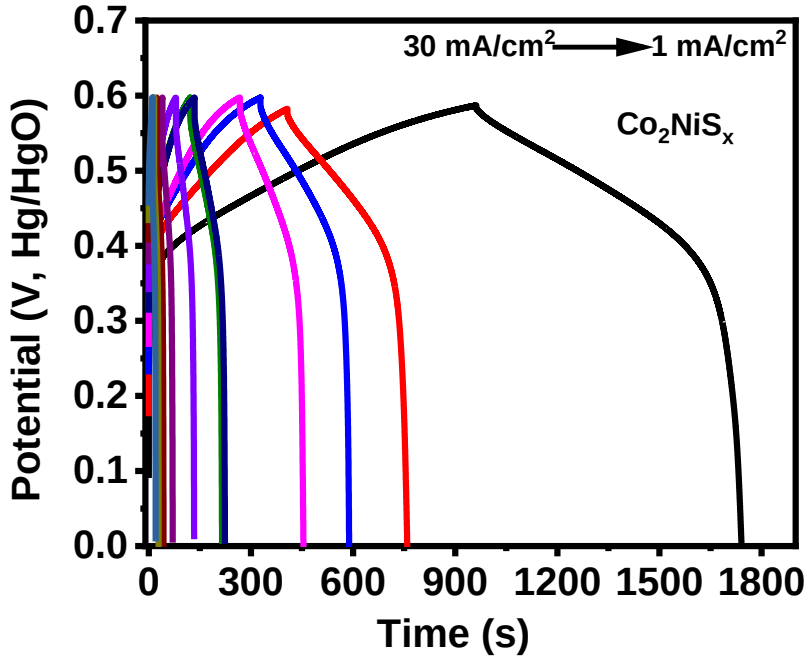

Figure 3.77. Potential versus time at different current density for Co_2NiS_X.

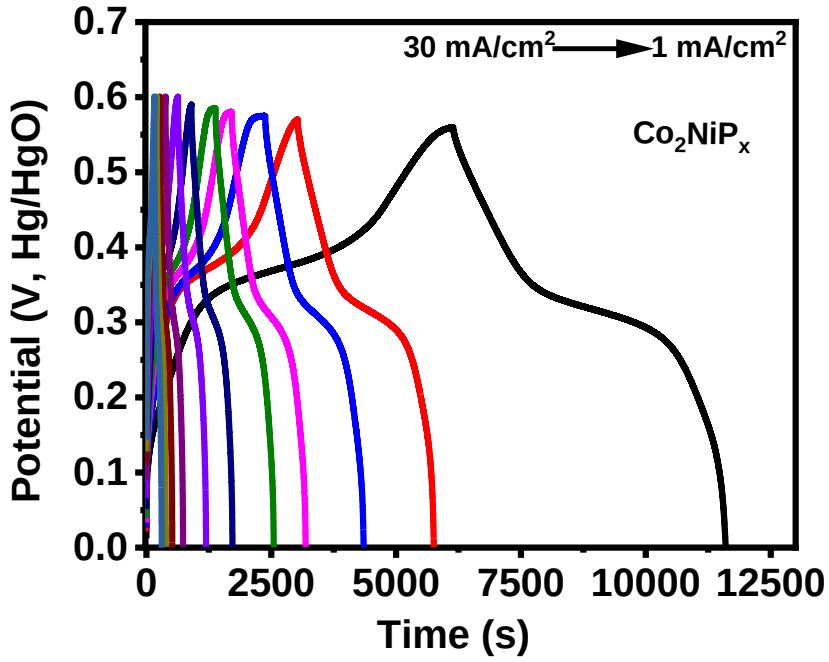

Figure 3.78. Potential versus time at different current density for Co_2NiP_X.

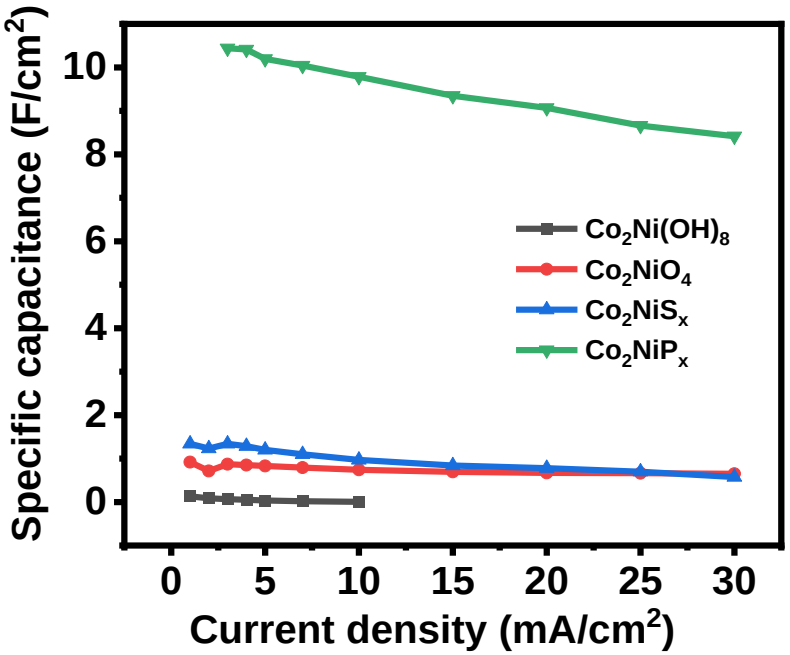

Figure 3.79. Specific capacitance versus current density for $Co_2Ni(OH)_8$, Co_2NiO_4, Co_2NiS_X, and Co_2NiP_X.

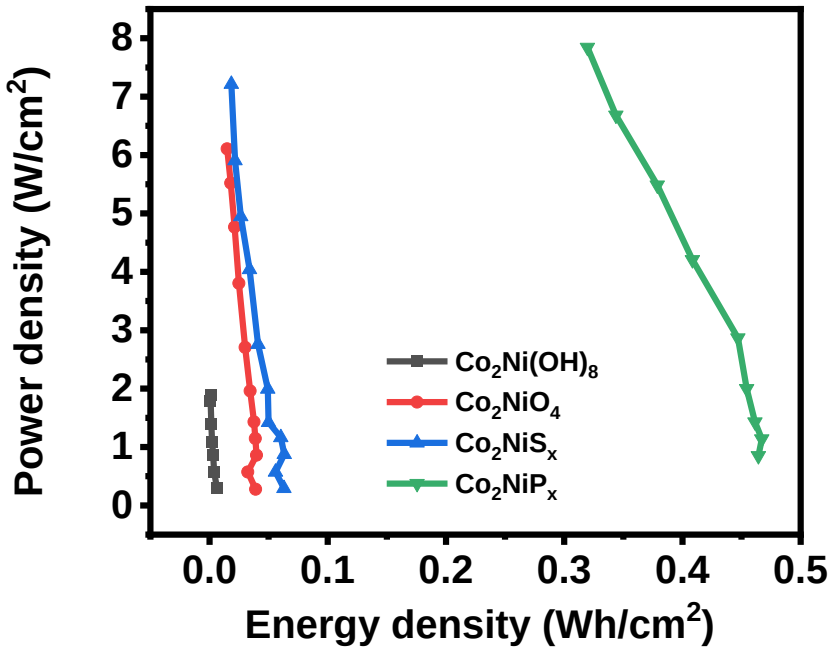

Figure 3.80. Power density versus energy density for $Co_2Ni(OH)_8$, Co_2NiO_4, Co_2NiS_X, and Co_2NiP_X.

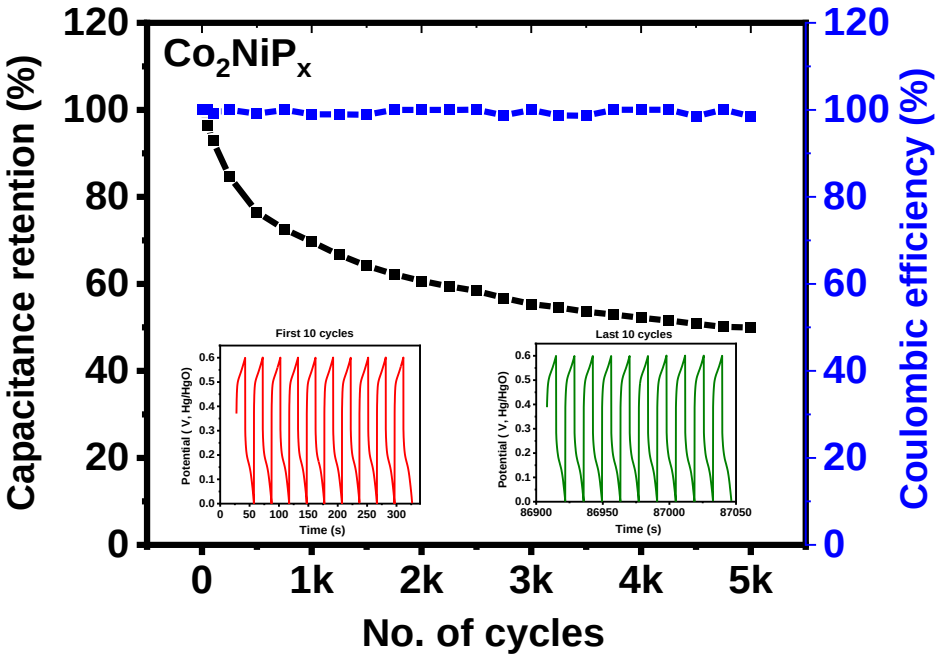

Figure 3.81. Stability curves for Co_2NiP_X.

CHAPTER IV

CONCLUSION

In conclusion, several different cobalt-nickel compounds have been successfully synthesized on nickel foam and carbon cloth by hydrothermal and electrodeposition synthesis methods, respectively. Scanning electron microscopy was used to reveal the microstructure of these materials. X-ray photoelectron spectroscopy was used to determine the composition and valence state of the synthesized compounds. The scale-like cobalt nickel phosphide (Co_2NiP_X@C) synthesized by the hydrothermal method exhibits excellent HER electrocatalytic activity with a very low overpotential of 48 mV at 10 mA/cm^2. In addition, Co_2NiP_X@C also has excellent pseudocapacitive energy storage performance, its specific capacitance is as high as 13.8 F/cm^2 at 0.5 mA/cm^2, up to 90% capacitance retention rate after 5000 charge-discharge cycles, and excellent rate performance. To simplify the synthesis process of Co_2NiP_X@C, Co_2NiP_X synthesized by electrode method on carbon cloth also has remarkable electrochemical properties. Co_2NiP_X shows ultra-high specific capacitance, 9.8 F/cm^2 at 1 A/cm^2. It is worth noting that the electrodes based on carbon cloth are flexible and have great value in the research and application of flexible electrodes.

REFERENCES

1. Sánchez-Bastardo Nuria, Schlögl Robert, Ruland Holger (2021) Methane Pyrolysis for Zero-Emission Hydrogen Production: A Potential Bridge Technology from Fossil Fuels to a Renewable and Sustainable Hydrogen Economy. Ind Eng Chem Res 60:11855–11881
2. Sun Yanzhi, Chang Cuiping, Zhu Silu, Liu Xingyu, Chen Yongmei, Tang Yang, Wan Pingyu, Pan Junqing (2021) One-step electrodeposition synthesis of bimetal fe-And co-doped NiPi/P for highly efficient overall water splitting. Ind Eng Chem Res 60:2070–2078
3. Kim Hyung Chul, Wallington Timothy J., Arsenault Renata, Bae Chulheung, Ahn Suckwon, Lee Jaeran (2016) Cradle-to-Gate Emissions from a Commercial Electric Vehicle Li-Ion Battery: A Comparative Analysis. Environ Sci Technol 50:7715–7722
4. He Ruijie, Zhao Zheng, Liu Pei, Li Zheng (2018) Transport Fuel Supply and Demand of the Passenger Car Sector in China up to 2030: A Modeling Approach. ACS Sustain Chem Eng 6:4633–4647
5. Jin Xiaoye, Li Meiying, Zhang Wanyu, Cui Jingwen, Meng Fansheng (2020) Factors Influencing the Development Ability of Intelligent Manufacturing of New Energy Vehicles Based on a Structural Equation Model. ACS Omega 5:18262–18272
6. Heligman Brian T., Manthiram Arumugam (2021) Elemental Foil Anodes for Lithium-Ion Batteries. ACS Energy Lett 6:2666–2672
7. Rey Irene, Vallejo Claudia, Santiago Gabriel, Iturrondobeitia Maider, Lizundia

Erlantz (2021) Environmental Impacts of Graphite Recycling from Spent Lithium-Ion Batteries Based on Life Cycle Assessment. ACS Sustain Chem Eng 9:14488–14501

8. Jena Kishore K., Alfantazi Akram, Mayyas Ahmad T. (2021) Comprehensive Review on Concept and Recycling Evolution of Lithium-Ion Batteries (LIBs). Energy and Fuels 35:18257–18284

9. Yuksel Tugce, Michalek Jeremy J. (2015) Effects of regional temperature on electric vehicle efficiency, range, and emissions in the united states. Environ Sci Technol 49:3974–3980

10. Weis Allison, Michalek Jeremy J., Jaramillo Paulina, Lueken Roger (2015) Emissions and cost implications of controlled electric vehicle charging in the U.S. PJM interconnection. Environ Sci Technol 49:5813–5819

11. Li Yuyang, Chang Guofeng, Xu Yiming, Zhang Jienan, Zhao Wang (2020) A Review of MHP Technology and Its Research Status in Cooling of Li-Ion Power Battery and PEMFC. Energy and Fuels 34:13335–13349

12. Pervez Syed Atif, Cambaz Musa Ali, Thangadurai Venkataraman, Fichtner Maximilian (2019) Interface in Solid-State Lithium Battery: Challenges, Progress, and Outlook. ACS Appl Mater Interfaces. https://doi.org/10.1021/acsami.9b02675

13. Zhu Guanjia, Chao Dongliang, Xu Weilan, Wu Minghong, Zhang Haijiao (2021) Microscale Silicon-Based Anodes: Fundamental Understanding and Industrial

Prospects for Practical High-Energy Lithium-Ion Batteries. ACS Nano 15:15567–15593

14. Salunkhe Rahul R., Kaneti Yusuf V., Yamauchi Yusuke (2017) Metal-Organic Framework-Derived Nanoporous Metal Oxides toward Supercapacitor Applications: Progress and Prospects. ACS Nano 11:5293–5308
15. Gao Haiwen, Shen Honglong, Wu Haoxuan, Jing Haiyan, Sun Yingxin, Liu Boyuan, Chen Ziyu, Song Juanjuan, Lu Longgang, Wu Zongdeng, Hao Qingli (2021) Review of Pristine Metal-Organic Frameworks for Supercapacitors: Recent Progress and Perspectives. Energy and Fuels 35:12884–12901
16. Bailey Alla, Andrews Lisa, Khot Ameya, Rubin Lea, Young Jun, Allston Thomas D., Takacs Gerald A. (2015) Hydrogen storage experiments for an undergraduate laboratory course-clean energy: Hydrogen/fuel cells. J Chem Educ 92:688–692
17. Stolbov Sergey, Alcántara Ortigoza Marisol (2012) Rational design of competitive electrocatalysts for hydrogen fuel cells. J Phys Chem Lett 3:463–467
18. Bora Mousumi, Bhattacharjya Dhrubajyoti, Saikia Binoy K. (2021) Coal-Derived Activated Carbon for Electrochemical Energy Storage: Status on Supercapacitor, Li-Ion Battery, and Li-S Battery Applications. Energy and Fuels 35:18285–18307
19. Shaikh Navajsharif S., Lokhande V. C., Praserthdam Supareak, Lokhande Chandrakant D., Ezema F. I., Salunkhe D. J., Shaikh Jasmin S., Kanjanaboos Pongsakorn (2021) Recent Advancements in Energy Storage Based on Sodium Ion and Zinc Ion Hybrid Supercapacitors. Energy and Fuels 35:14241–14264

20. Kumar Kowsik Sambath, Choudhary Nitin, Jung Yeonwoong, Thomas Jayan (2018) Recent Advances in Two-Dimensional Nanomaterials for Supercapacitor Electrode Applications. ACS Energy Lett 3:482–495

21. Karade Swapnil S., Sankapal Babasaheb R. (2018) Materials Mutualism through EDLC-Behaved MWCNTs with Pseudocapacitive MoTe2 Nanopebbles: Enhanced Supercapacitive Performance. ACS Sustain Chem Eng 6:15072–15082

22. Jeanmairet Guillaume, Rotenberg Benjamin, Salanne Mathieu (2022) Microscopic Simulations of Electrochemical Double-Layer Capacitors. Chem Rev acs.chemrev.1c00925

23. You Xiangyu, Misra Manjusri, Gregori Stefano, Mohanty Amar K. (2018) Preparation of an Electric Double Layer Capacitor (EDLC) Using Miscanthus-Derived Biocarbon. ACS Sustain Chem Eng 6:318–324

24. Shao Yuanlong, El-Kady Maher F., Sun Jingyu, Li Yaogang, Zhang Qinghong, Zhu Meifang, Wang Hongzhi, Dunn Bruce, Kaner Richard B. (2018) Design and Mechanisms of Asymmetric Supercapacitors. Chem. Rev. 118:9233–9280

25. Chen Kunfeng, Yang Yangyang, Li Keyan, Ma Zengsheng, Zhou Yichun, Xue Dongfeng (2014) CoCl2 designed as excellent pseudocapacitor electrode materials. ACS Sustain Chem Eng 2:440–444

26. Seok Jae Young, Lee Jaehak, Yang Minyang (2018) Self-Generated Nanoporous Silver Framework for High-Performance Iron Oxide Pseudocapacitor Anodes. ACS Appl Mater Interfaces 10:17223–17231

27. Ke Shan Chao, Chen Rui, Chen Gang Hua, Ma Xue Liang (2021) Mini Review on Electrocatalyst Design for Seawater Splitting: Recent Progress and Perspectives. Energy and Fuels 35:12948–12956

28. Uddin Md Nasir, Daud W. M.A.Wan (2014) Technological diversity and economics: Coupling effects on hydrogen production from biomass. In: Energy and Fuels. American Chemical Society, pp 4300–4320

29. Ganapathy Mano, Hsu Yang, Thomas Joy, Chen Liang Yih, Chang Chang Tang, Alagan Viswanathan (2021) Preparation of SrTiO3/Bi2S3Heterojunction for Efficient Photocatalytic Hydrogen Production. Energy and Fuels 35:14995–15004

30. Bolt Andre, Dincer Ibrahim, Agelin-Chaab Martin (2021) A Review of Unique Aluminum-Water Based Hydrogen Production Options. Energy and Fuels 35:1024–1040

31. Ding Dianjin, Huang Jinzhao, Deng Xiaolong, Fu Ke (2021) Recent Advances and Perspectives of Nanostructured Amorphous Alloys in Electrochemical Water Electrolysis. Energy and Fuels 35:15472–15488

32. Zhang Feifei, Wang Qing (2021) Redox-Mediated Water Splitting for Decoupled H2Production. ACS Mater. Lett. 3:641–651

33. Yan Ya, Xia Baoyu, Xu Zhichuan, Wang Xin (2014) Recent development of molybdenum sulfides as advanced electrocatalysts for hydrogen evolution reaction. ACS Catal. 4:1693–1705

34. Zhu Qing, Qu Yuanju, Liu Detao, Ng Kar Wei, Pan Hui (2020) Two-Dimensional

Layered Materials: High-Efficient Electrocatalysts for Hydrogen Evolution Reaction. ACS Appl Nano Mater 3:6270–6296

35. Yang Dong Hui, Tao You, Ding Xuesong, Han Bao Hang (2022) Porous organic polymers for electrocatalysis. Chem Soc Rev 51:761–791

36. Feng Chao, Faheem M. Bilal, Fu Jie, Xiao Yequan, Li Changli, Li Yanbo (2020) Fe-Based Electrocatalysts for Oxygen Evolution Reaction: Progress and Perspectives. ACS Catal 10:4019–4047

37. Ding Hui, Liu Hongfei, Chu Wangsheng, Wu Changzheng, Xie Yi (2021) Structural Transformation of Heterogeneous Materials for Electrocatalytic Oxygen Evolution Reaction. Chem. Rev. 121:13174–13212

38. Zhang Wei, Lai Wenzhen, Cao Rui (2017) Energy-Related Small Molecule Activation Reactions: Oxygen Reduction and Hydrogen and Oxygen Evolution Reactions Catalyzed by Porphyrin- and Corrole-Based Systems. Chem. Rev. 117:3717–3797

39. Sivanantham Arumugam, Ganesan Pandian, Vinu Ajayan, Shanmugam Sangaraju (2020) Surface Activation and Reconstruction of Non-Oxide-Based Catalysts through in Situ Electrochemical Tuning for Oxygen Evolution Reactions in Alkaline Media. ACS Catal. 10:463–493

40. Lellala Kashinath (2021) Microwave-Assisted Facile Hydrothermal Synthesis of Fe3O4-GO Nanocomposites for the Efficient Bifunctional Electrocatalytic Activity of OER/ORR. Energy and Fuels 35:8263–8274

41. Meng Tao, Cao Minhua (2020) Interfacial Electronic and Structural Reorganization in Mn2Co2C/MnO for Enhancing Oxygen Evolution Kinetics and Active Sites. ACS Sustain Chem Eng 8:13271–13281

42. Esquius Jonathan Ruiz, Algara-Siller Gerardo, Spanos Ioannis, Freakley Simon J., Schlögl Robert, Hutchings Graham J. (2020) Preparation of solid solution and layered Irox−Ni(OH)2 oxygen evolution catalysts: Toward optimizing iridium efficiency for OER. ACS Catal 10:14640–14648

43. Wang Cheng, Xu Hui, Wang Yuan, Shang Hongyuan, Jin Liujun, Ren Fangfang, Song Tongxin, Guo Jun, Du Yukou (2020) Hollow V-Doped CoMx(M = P, S, O) Nanoboxes as Efficient OER Electrocatalysts for Overall Water Splitting. Inorg Chem 59:11814–11822

44. Mathankumar Mahendran, Karthick Kannimuthu, Nanda Kumar Amal Kaitheri, Kundu Subrata, Balasubramanian Subramanian (2021) In Situ Decorated Ni Metallic Layer with CoS2-Layered Thin Films via a Layer-by-Layer Strategy Using Pulsed Laser Deposition for Enhanced Electrocatalytic OER. Inorg Chem 60:8946–8957

45. Cao Lujie, Cao Lujie, Shao Yangfan, Shao Yangfan, Pan Hui, Lu Zhouguang (2020) Designing Efficient Dual-Metal Single-Atom Electrocatalyst TMZnN6(TM = Mn, Fe, Co, Ni, Cu, Zn) for Oxygen Reduction Reaction. J Phys Chem C 124:11301–11307

46. Wu Jason, Park Hey Woong, Yu Aiping, Higgins Drew, Chen Zhongwei (2012) Facile synthesis and evaluation of nanofibrous iron-carbon based non-precious

oxygen reduction reaction catalysts for Li-O 2 battery applications. J Phys Chem C 116:9427–9432

47. Ha Yuan, Shi Lingxia, Yan Xiaoxiao, Chen Ziliang, Li Yunpeng, Xu Wei, Wu Renbing (2019) Multifunctional Electrocatalysis on a Porous N-Doped NiCo2O4@C Nanonetwork. ACS Appl Mater Interfaces 11:45546–45553

48. Li Zesheng, Li Bolin, Hu Yifan, Wang Shaoyu, Yu Changlin (2022) Highly-dispersed and high-metal-density electrocatalysts on carbon supports for the oxygen reduction reaction: from nanoparticles to atomic-level architectures. Mater Adv 3:779–809

49. Zhang Rui, Wang Xiangxue, Yu Shujun, Wen Tao, Zhu Xiangwei, Yang Fangxu, Sun Xiangnan, Wang Xiangke, Hu Wenping (2017) Ternary NiCo2Px Nanowires as pH-Universal Electrocatalysts for Highly Efficient Hydrogen Evolution Reaction. Adv Mater 29:

50. Zhou Lei, Jiang Shan, Liu Yunke, Shao Mingfei, Wei Min, Duan Xue (2018) Ultrathin CoNiP@Layered Double Hydroxides Core-Shell Nanosheets Arrays for Largely Enhanced Overall Water Splitting. ACS Appl Energy Mater 1:623–631

51. Du Cheng, Yang Lan, Yang Fulin, Cheng Gongzhen, Luo Wei (2017) Nest-like NiCoP for Highly Efficient Overall Water Splitting. ACS Catal 7:4131–4137

52. Tian Yumeng, Lin Zaiwen, Yu Jing, Zhao Sijia, Liu Qi, Liu Jingyuan, Chen Rongrong, Qi Yunfei, Zhang Hongsen, Li Rumin, Li Junqing, Wang Jun (2019) Superaerophobic Quaternary Ni-Co-S-P Nanoparticles for Efficient Overall Water-

Splitting. ACS Sustain Chem Eng 7:14639–14646

53. Gao Di, Guo Jiangna, Cui Xun, Yang Lin, Yang Yang, He Huichao, Xiao Peng, Zhang Yunhuai (2017) Three-Dimensional Dendritic Structures of NiCoMo as Efficient Electrocatalysts for the Hydrogen Evolution Reaction. ACS Appl Mater Interfaces 9:22420–22431

54. Liu Hui, Ma Xiao, Hu Han, Pan Yuanyuan, Zhao Weinan, Liu Jialiang, Zhao Xinyu, Wang Jialin, Yang Zhongxue, Zhao Qingshan, Ning Hui, Wu Mingbo (2019) Robust NiCoP/CoP Heterostructures for Highly Efficient Hydrogen Evolution Electrocatalysis in Alkaline Solution. ACS Appl Mater Interfaces 11:15528–15536

55. Yan Xiaodong, Tian Lihong, He Min, Chen Xiaobo (2015) Three-Dimensional Crystalline/Amorphous Co/Co3O4 Core/Shell Nanosheets as Efficient Electrocatalysts for the Hydrogen Evolution Reaction. Nano Lett 15:6015–6021

56. Zhang Tao, Sun Yiqiang, Hang Lifeng, Bai Yu, Li Xinyang, Wen Lulu, Zhang Xiaomin, Lyu Xianjun, Cai Weiping, Li Yue (2018) Large-Scale Synthesis of Co/CoOx Encapsulated in Nitrogen-, Oxygen-, and Sulfur-Tridoped Three-Dimensional Porous Carbon as Efficient Electrocatalysts for Hydrogen Evolution Reaction. ACS Appl Energy Mater 1:6250–6259

57. Tong Rui, Sun Zhi, Zhang Fang, Wang Xina, Xu Jincheng, Shi Xingqiang, Wang Shuangpeng, Pan Hui (2018) N and v Coincorporated Ni Nanosheets for Enhanced Hydrogen Evolution Reaction. ACS Sustain Chem Eng 6:16525–16531

58. Li Zhenxing, Yu Chengcheng, Wen Yangyang, Gao Yang, Xing Xiaofei, Wei Zhiting,

Sun Hui, Zhang Ya Wen, Song Weiyu (2019) Mesoporous Hollow Cu-Ni Alloy Nanocage from Core-Shell Cu@Ni Nanocube for Efficient Hydrogen Evolution Reaction. ACS Catal 9:5084–5095

59. Theerthagiri Jayaraman, Cardoso Eduardo S.F., Fortunato Guilherme V., Casagrande Gleison A., Senthilkumar Baskar, Madhavan Jagannathan, Maia Gilberto (2019) Highly Electroactive Ni Pyrophosphate/Pt Catalyst toward Hydrogen Evolution Reaction. ACS Appl Mater Interfaces 11:4969–4982

60. Abdelkader-Fernández Víctor K., Fernandes Diana M., Balula Salete S., Cunha-Silva Luís, Pérez-Mendoza Manuel José, López-Garzón F. Javier, Pereira M. Fernando, Freire Cristina (2019) Noble-Metal-Free MOF-74-Derived Nanocarbons: Insights on Metal Composition and Doping Effects on the Electrocatalytic Activity Toward Oxygen Reactions. ACS Appl Energy Mater 2:1854–1867

61. Wang Jingjing, Zeng Hua Chun (2020) Hybrid OER Electrocatalyst Combining Mesoporous Hollow Spheres of N, P-Doped Carbon with Ultrafine Co2NiOx. ACS Appl Mater Interfaces 12:50324–50332

62. Wang Wenquan, Xi Shunming, Shao Yalong, Sun Wenhao, Wang Shikun, Gao Jiafei, Mao Changming, Guo Xiaosong, Li Guicun (2019) Oxide Passivated CoNi@NC-Supported Ru(OH)xCly Cluster as Highly Efficient Catalysts for the Oxygen and Hydrogen Evolution. ACS Sustain Chem Eng 7:17227–17236

63. Ren Baiyu, Zhang Bao Yue, Zhang Haitao, Jiang Xinglin, Yi Qian, Xu Kai, Yu Hao, Hu Zhangmei, Jeerapan Itthipon, Ou Jian Zhen (2022) CoNi Layered Double Hydroxide

Nanosheets Vertically Grown on Electrodeposited Dendritic Copper Substrates for Supercapacitor Applications. ACS Appl Nano Mater 5:2395–2404

64. Ai Yuanfei, Geng Xuewen, Lou Zheng, Wang Zhiming M., Shen Guozhen (2015) Rational Synthesis of Branched CoMoO4@CoNiO2 Core/Shell Nanowire Arrays for All-Solid-State Supercapacitors with Improved Performance. ACS Appl Mater Interfaces 7:24204–24211

65. Wan Lian, Xiao Junwu, Xiao Fei, Wang Shuai (2014) Nanostructured (Co, Ni)-based compounds coated on a highly conductive three dimensional hollow carbon nanorod array (HCNA) scaffold for high performance pseudocapacitors. ACS Appl Mater Interfaces 6:7735–7742

66. Zhang Jian, Liu Xiaoxi, Yin Qing, Zhao Yajun, Luo Jianeng, Han Jingbin (2019) CoNi2S4 Nanoplate Arrays Derived from Hydroxide Precursors for Flexible Fiber-Shaped Supercapacitors. ACS Omega 4:11863–11870

67. Tian Rongrong, Duan Chengyuan, Feng Yi, Cao Mengjue, Yao Jianfeng (2021) Metal Organic Framework-Based CoNi Composites on Carbonized Wood as Advanced Freestanding Electrodes for Supercapacitors. Energy and Fuels 35:4604–4608

68. Zhang Nan, Li Yifan, Xu Junyuan, Li Junjie, Wei Bin, Ding Yu, Amorim Isilda, Thomas Rajesh, Thalluri Sitaramanjeneya Mouli, Liu Yuanyue, Yu Guihua, Liu Lifeng (2019) High-Performance Flexible Solid-State Asymmetric Supercapacitors Based on Bimetallic Transition Metal Phosphide Nanocrystals. ACS Nano

13:10612–10621

69. Wang Yanzhong, Liu Yuexin, Wang Huiqi, Liu Wei, Li Ying, Zhang Jinfang, Hou Hua, Yang Jinlong (2019) Ultrathin NiCo-MOF Nanosheets for High-Performance Supercapacitor Electrodes. ACS Appl Energy Mater 2:2063–2071

70. Chen Hongyuan, Cai Feng, Kang Yiran, Zeng Sha, Chen Minghai, Li Qingwen (2014) Facile assembly of Ni-Co hydroxide nanoflakes on carbon nanotube network with highly electrochemical capacitive. ACS Appl Mater Interfaces 6:19630–19637

71. Xiang Cuili, Liu Yin, Yin Ying, Huang Pengru, Zou Yongjin, Fehse Marcus, She Zhe, Xu Fen, Banerjee Dipanjan, Hermida Merino Daniel, Longo Alessandro, Kraatz Heinz Bernhard, Brougham Dermot F., Wu Bing, Sun Lixian (2019) Facile Green Route to Ni/Co Oxide Nanoparticle Embedded 3D Graphitic Carbon Nanosheets for High Performance Hybrid Supercapacitor Devices. ACS Appl Energy Mater 2:3389–3399

72. Chu Wenjing, Shi Zijun, Hou Yongdan, Ma Dongni, Bai Xue, Gao Yanfang, Yang Nianjun (2020) Trifunctional of Phosphorus-Doped NiCo2O4 Nanowire Materials for Asymmetric Supercapacitor, Oxygen Evolution Reaction, and Hydrogen Evolution Reaction. ACS Appl Mater Interfaces 12:2763–2772